NAM Nederlandse Aardolie Maatschappij B.V.

Inspecteur-Generaal der Mijnen

T.a.v. drs. H.A.J.M. van der Meijden

Postbus 24037

2490 AA DEN HAAG

Brief ref.: EP201610210372

Datum: 28 oktober 2016

Onderwerp: **Norg ondergrondse gasopslag – Opslagplan**

Bij besluit van 6 augustus 2015, kenmerk DGETM-EO/15103827, is ingestemd met een wijziging van het opslagplan voor de ondergrondse gasopslag Norg. Hierbij zijn een aantal aanvullende voorwaarden en beperkingen gesteld.

Bijgevoegd is het rapport "Norg UGS fault reactivation study and implications for seismic threat" waarmee invulling wordt gegeven aan artikel 11 van dit besluit waarin wordt voorgeschreven dat NAM voor 1 november 2016 een schriftelijke update moet aanleveren van de seismische risicoanalyses voor de UGS Norg gebaseerd op de waargenomen seismiciteit en een geactualiseerd geomechanisch model, waarin specifiek aandacht gegeven wordt aan de randbreuken van compartiment 2.

Hoogachtend,

Nederlandse Aardolie Maatschappij B.V.

Ir. J. de Haan

Asset Manager Groningen

Subsurface technical report

Norg UGS fault reactivation study and implications for seismic threat

Date: October, 2016 Document Number: EP201610208045

NEDERLANDSE AARDOLIE MAATSCHAPPIJ B.V. ASSEN

Summary

This report investigates the potential of fault reactivation and possible related seismicity of the block 2 boundary faults in the Norg field over its production and storage lifetime with an outlook to the future where NAM will request for larger cycling volumes in a new "opslagplan". The report is the response to a condition (article 11) stated in the approval of the UGS Norg Opslagplan by the Ministry of Economic Affairs[1].

This study is based on field observations, laboratory measurements and a geomechanical assessment of the fault stability. The main field observation comprise

- Only two small events on boundary faults have been observed over the whole operational period of the Norg UGS
- no seismicity was observed over the last 17 years despite the high variation of production- and injection (rates)
- High permeability of the reservoir rock and therefore no relative pressure build-up in the fault plane
- Small temperature differences between the injected gas and reservoir rock
- Production and injection rates do not show an obvious correlation with seismicity
- Low ambient shear stress level observed from the in-situ Norg leak-off test

Laboratory measurements show that irrecoverable deformations may accumulate, while the stress paths are reversible in most tests. This is in correspondence with surface deformation monitoring. A different stress path under re-pressurisation compared to depletion would be the main mechanism that could lead to increased seismic risk.

The objective of the numerical study is to formulate an expectation for future seismic activity based on geomechanical principles. To this end, two mechanisms for developing a different stress path under depletion and re-pressurisation have been evaluated for the two seismic locations in the Norg UGS. A-seismic fault slip is considered to be the main source for the development of a different stress path. The results suggest low fault strength in combination with relative ductile fault slip behaviour. If any, fault slip must have occurred a-seismically in view of the absence of seismic events over the last 17 years.

Therefore, based on field observations, laboratory measurements and model hypothesis, current expectation is that stress paths will remain (virtually) the same under depletion and re-pressurisation and that the likelihood of seismic events is small within the entire historical reservoir pressure range.

[1] https://zoek.officielebekendmakingen.nl/stcrt-2015-24945.html

Contents

1 Introduction

This report investigates the potential of fault reactivation and possible related seismicity of the block 2 boundary faults (blue part of the field in Figure 1) in the Norg field over its historic production and storage lifetime with an outlook to the future where NAM will request approval of a new "opslagplan" to operate the Norg UGS with larger cycling volumes and consequently larger pressure ranges. This investigation is part of a condition in the approval of the UGS Norg Opslagplan (article 11) by the Ministry of Economic Affairs[2].

There are four underground gas storage (UGS) sites in the Netherlands. The Bergermeer and Alkmaar sites are operated by Taqa, while the Grijpskerk and Norg sites are operated by NAM. All sites except Alkmaar showed some level of seismicity during the depletion phase of the field (TNO, 2015) where the Bergermeer site experienced 3 earthquakes above a local magnitude value of 3.0. The Norg and Grijpskerk sites only showed four small (Ml≤ 1.5) events over their operational lifetime. None of these events were reported to be felt by anyone. Figure 1 shows a base Zechstein map that can be considered as the top structure map of the reservoir layer. The Norg UGS is surrounded by other gas fields with high levels of depletion without observing high seismic activity and/or high magnitude values. The largest registered earthquake (Ml=2.1) is located at the edge of the Roden field. There are no claims or reports of damage because of any event in this region.

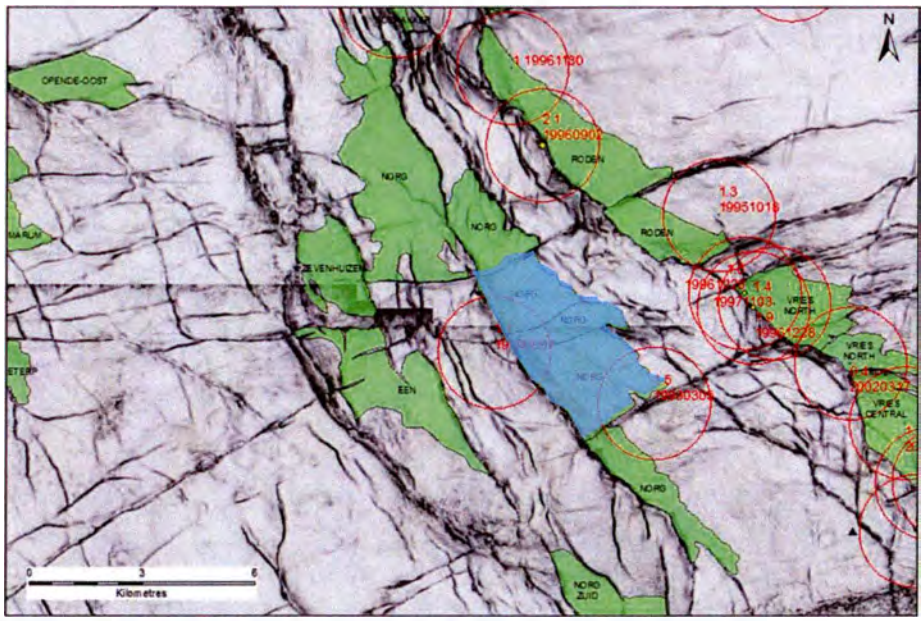

Figure 1 Base Zechstein semblance map of the Norg UGS and surrounding area.

[2] https://zoek.officielebekendmakingen.nl/stcrt-2015-24945.html

Nagelhout and Roest (1997) investigated for NAM the possibility of fault slip due to the production and injection of natural gas in Norg before the start of the UGS project. Their focus was on the internal NW-SE faults in block 2 with the following main conclusions and with a comparison to the observations since then in *italic*:

1. "During depletion, compaction of the reservoir occurs. This induces slip on the intra reservoir faults." *According to the current observations, it is more likely that the boundary faults have slipped.*
2. "When cycling gas, a very limited amount of additional slip is observed at the intra reservoir faults." *This point is confirmed by the observations or more precisely by the lack of observed seismicity.*
3. "There is a limited risk of faults in the shallow overburden being triggered, but it is not expected to increase when cycling gas." *This point is confirmed by the lack of observed seismicity in the overburden over the last 17 years.*
4. "The numerical modelling complies with poroelastic theories describing the response of the reservoir when varying the pore pressure." *Poroelastic theory is still the basis to assess effective stresses. However, irrecoverable (plastic) deformations during the first phase of depletion is confirmed by both laboratory and field observations.*

To summarize, the model of Nagelhout and Roest predicts limited seismic activity that is confirmed by the lack of observed seismicity since 1999. There is however a difference in the position of the epicentres of the two earthquakes in their study compared to the latest KNMI location of these earthquakes[3] (Figure 2). The Ml=2.1, 19960902 earthquake is now allocated to a different field (Roden) while the epicentre of the Ml=1.5 earthquake shifted from the central part of the block 2 reservoir towards the southern boundary fault of block 2. This observations leads to the current conclusion that the boundary faults are most prone for reactivation and not the internal faults as claimed in study by Nagelhout and Roest.

[3] http://www.knmi.nl/nederland-nu/seismologie/aardbevingen

Location	Date	Co-ordinates (Amersfoort)	Intensity (Mod. Merc.)	Magnitude (M_l)	Depth (km)
Langelo	5-3-1993	568.2; 225.2	II - III	1.5	-
Nieuw Roden	2-9-1996	572.6; 222.6	III - IV	2.1	2.5

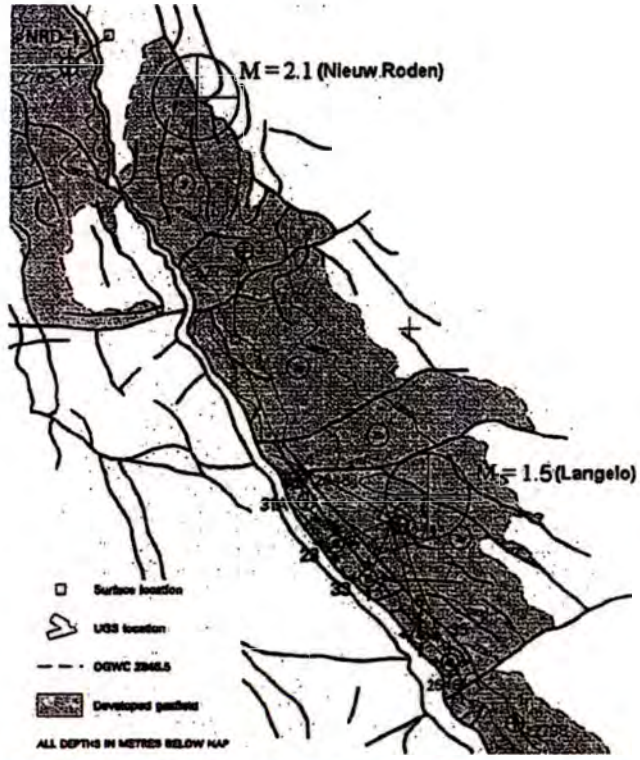

Figure 2 Field map of Norg and the locations of the two earthquakes as presented by Nagelhout and Roest (1997). The coordinates are different when compared to the current catalogue.

Details of these two locations using the latest information from KNMI are listed in Table 1. The uncertainty of the location of the small events is relative large (1500m). Location and uncertainty of the epicentres are visualised as well in Figure 1.

Table 1 Locations, date and magnitude of seismic events occurred in the Norg Field

	RD x (m)	RD y (m)	Datum YYYYMMDD	M_l
Langelo	227234	566874	19930305	1.5
Steenbergen	222942	568315	19990607	1.1

2 Geology of the Norg UGS

2.1 Norg Field Rotliegend Structure

The Norg field covers a surface area of approximately 30 km^2, lying along a NW-SE trending fault (Figure 3) on the western flank of the Lauwerszee Trough, a NW-SE structure to the west of the Groningen high. The trapping mechanism is structural, by the juxtaposition of the Rotliegend reservoir against a thick Zechstein evaporitic section to the west. The Norg Main Fault shows a quite consistent geometry (Figure 4) and reaches a maximum fault throw of 350m on the central portion

of the structure (Figure 5). The Norg structure is dip-closed and filled to spill point, with an original GWC at 2847 m TVNAP.

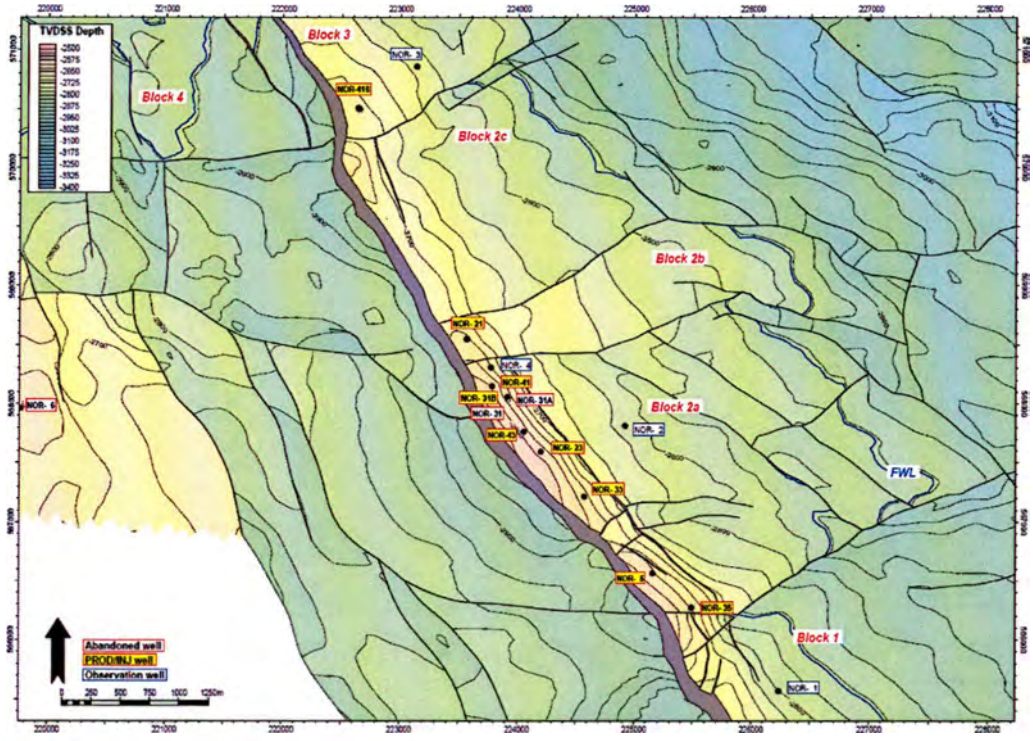

Figure 3 Top Reservoir depth map (m TVDSS)

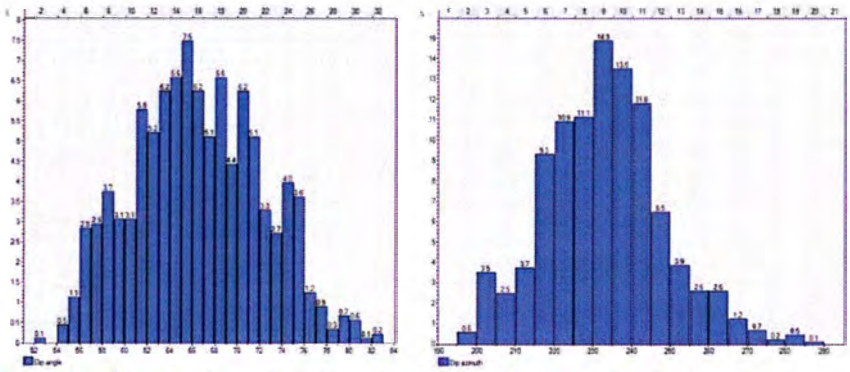

Figure 4 Dip and azimuth histograms for the Norg Main Bounding Fault.

The field can be subdivided into four structural blocks, from south to north (Figure 3):

- Block 1 in the south of the field, drilled by NOR-1 and separated from the rest of the field by a SW-NE fault.
- Block 2 contains most of the GIIP and is where most of the UGS operations are focused. From a structural point of view, this block is controlled by a pop-up structure that uplifts the crestal part of the block. Additionally, minor SW-NE faults separate 3 different sub-blocks.
- Block 3 in the north of the field (appraised by NOR-3)

- To the North, the Norg main field spills into Block 4 to the NW of the field (appraised by exploration well NRD-1).

2.2 Faulting and Block Communication

Faults over the Norg field are nearly vertical, with a significant normal component. Most of the faults offsetting the Rotliegend and basal Zechstein sediments die out in the Zechstein salt above the ZEZ2A anhydrite; exceptions include major faults such as the Norg main boundary fault, which penetrates through to shallower stratigraphic levels.

Three main fault families have been recognised within the Rotliegend from 3D seismic mapping:

- NW-SE trending extensional faults,
- SW-NE trending extensional faults, and
- NW-SE inversion related transpressional/compressional faults present along the crest of Norg block 2

Considering dynamic information, it is clear that the faults within the Norg Field are not sealing and that blocks 1, 2 and 3 are in pressure communication. Pressure communication between the main field and block 4 (drilled by NRD-1) has been inferred from the almost 90 bar pressure depletion encountered by the well and by the similar GWC and gas compositions.

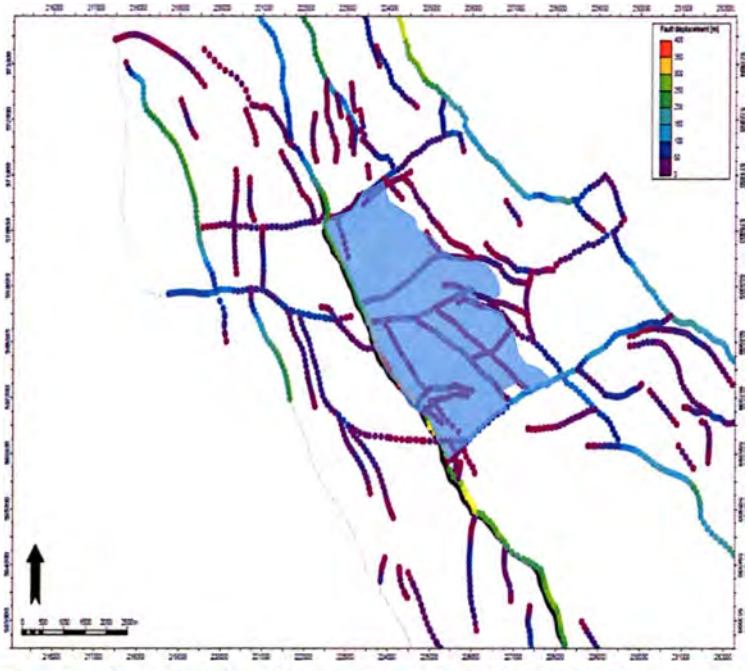

Figure 5 Norg Field fault throw map. The blue transparent area indicates the position of the Norg block 2

2.2.1 Reservoir properties and sedimentology

The Rotliegend in Norg is characterized by good reservoir properties, given its relatively proximal position in the basin, with high N/G and excellent reservoir quality and thicknesses ranging from 150m in the S to 200 m in the N. Average Reservoir properties for Norg field are listed in Table 2.

Table 2 Average Reservoir properties for Ten Boer & Slochteren members

	Ten Boer (RESU 1-2)	Slochteren(RESU 3-8)
Max HC column (m)	54	139
Net to Gross (%)	61	95
Porosity (%)	13	17
Sg (%)	69	72
Permeability (mD)	70	740

The stratigraphy of the Norg Field is typical for the North-East Netherlands. A representative cross-section over the field, including the overburden section, is displayed in Figure 6.

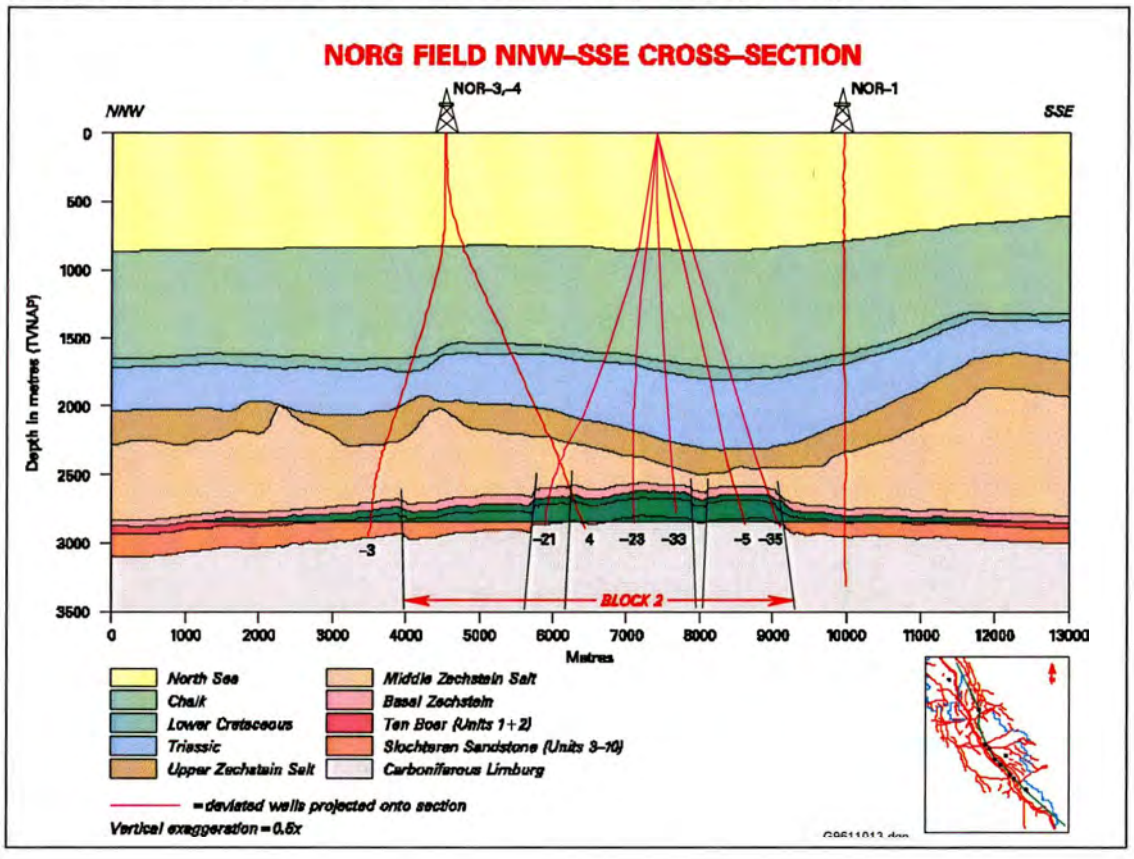

Figure 6 Regional Cross-section along the crest of the Norg structure

The Rotliegend was deposited at the southern margin of the Permian Basin in a fluvio/aeolian/desert lake environment. The contact with the underlying Carboniferous is known as the Saalian Unconformity. Climatic factors controlled the presence and lateral extension of fluvial facies in the

south of the basin and the progradation/retrogradation of the lacustrine system to the north. Periods of high precipitation resulted in an expansion of the lake system, reaching its maximum extension at the time of deposition of the Ameland Mb. Tectonic activity did not play a major role during the deposition of the Slochteren Mb. Basal units are characterized by the presence of fluvial/alluvial facies, evolving progressively to aeolian dominated facies and in a later stage to lacustrine dominated facies, during the time of the Ten Boer Mb equivalent RESU 1 & RESU 2.

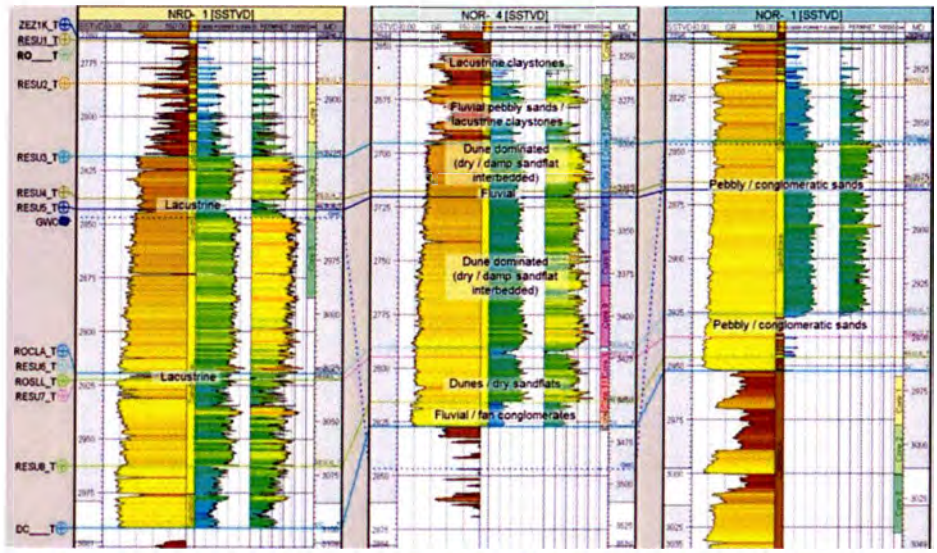

Figure 7 Reservoir Subdivision and sedimentological interpretation of the main reservoir zones

The lowermost reservoir unit (RESU8) is part of the Lower Slochteren Member and consist of fluvial and/or fan conglomerate deposits. This unit shows relatively low porosities, when compared with the rest of the Slochteren, and shows a progressive thinning toward the South of the field. The overlying reservoir unit (RESU7) is dominated by aeolian sand deposits (dunes and dry sandflats) with good reservoir properties. The Ameland Claystone Member above (RESU6) is developed as a clay-rich lacustrine deposit in the north and grades into a fluvial pebbly/conglomeratic sand unit towards the south of the Norg field. This shale-conglomerate correlation of RESU6 follows from the assumption that the Ameland Member has been deposited under relatively high rainfall conditions. This provoked the progradation of a fluvial system in the south because of an increase in run-off and, at the same time, the transgression of the desert lake to the north because of a rise in lake level.

Reservoir units 3, 4 and 5 form the Upper Slochteren Member and comprise a high net-to-gross dune-dominated sand sequence, interbedded with dry and damp sand-flat deposits.

RESU4 is a relatively thin fluvial sand (occasionally pebbly) unit towards the top of the Upper Slochteren and can be traced throughout the field. A sequence of fluvial pebbly sands and lacustrine/pond claystone beds conformably overlie the Slochteren Formation and characterise the basal part of the Ten Boer Claystone Member (RESU2). The overlying RESU1 is dominated by lacustrine claystones with fluvial, thinly bedded intercalations of sands and pebbly sands. The top Ten Boer Member is a sharp contact with the overlying Copper Shale (ZEZ1K), the basal unit of the Zechstein Group.

2.2.2 Cross-sections

16 cross sections are presented in Enclosure-1:

- One set of SW-NE cross sections perpendicular to the Norg Main Bounding Fault (Cross sections 1-13)
- One set of NW-SE cross sections perpendicular to the fault separating blocks 1 & 2 (Cross section 14-16)

Cross sections 1 to 13 illustrate the geometrical evolution from South to north of the Norg Main bounding fault (Labelled as Fault 1 in the cross sections), which reaches a maximum displacement of 350m to the center of the field, in block 2A. This structure evolves to the N (sections 11 to 13) to a compressive structure dipping to the west, opposite to the main Norg Field.

Cross sections 14 to 16 show the evolution of fault separating blocks 1 & 2 (Labelled as Fault 2 in the cross sections) Displacement along this fault increases to the east, but fault throw is lower than the total Rotliegend thickness, and therefore, this fault does not constitute a barrier to pressure communication in Norg.

3 Field data used in this study

3.1 Pressure data

The historical pressure in the Norg field is shown in Figure 8. The pressure history in Block 2 is of most interest, because this is the block with most pressure fluctuations as a result of the storage and production operations, and also because the two previously recorded seismic events are located at fault at the boundary of this block.

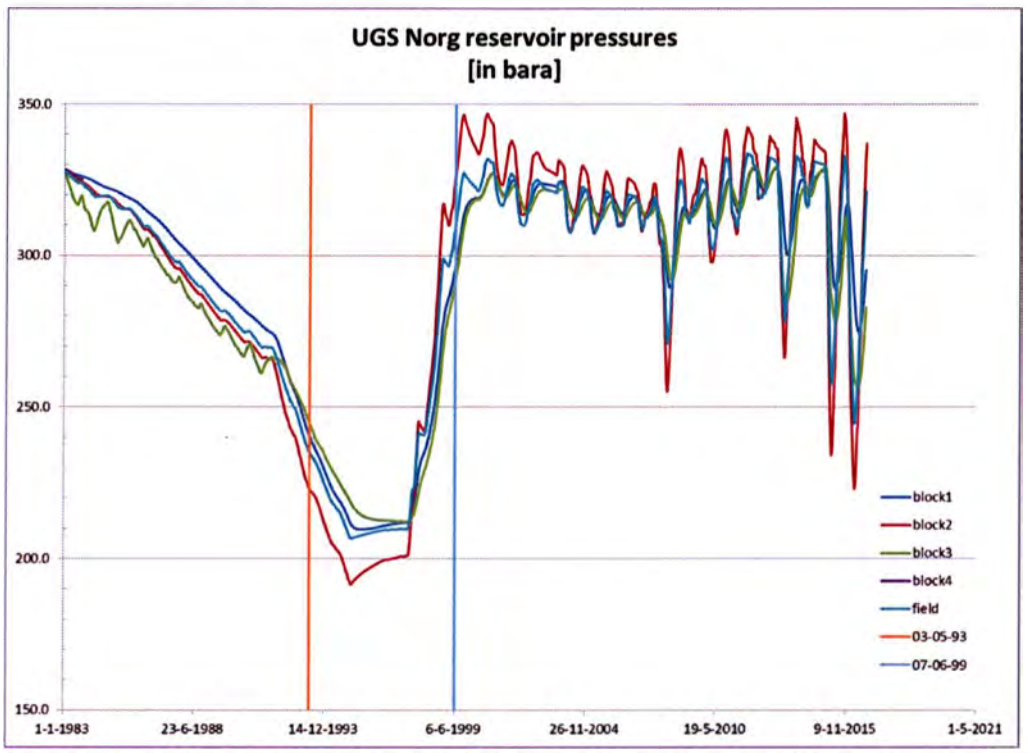

Figure 8 The average pressure per block, and for the entire field as a function of time. The two seismic events associated with the Norg field are indicated by the vertical lines.

The virgin average pressure (1 January 1983) in Block 2 is 327 bar. The minimum average pressure of around 190 bar was recorded on 31 January 1995, while the maximum average pressure of 347 bar was recorded on 26 September 2015. Furthermore, the average pressure in Block 2 is estimated at around 225 bar at the time of the first seismic event on 5 March 1993. The average pressure is estimated at 325 bar on 7 June 1999, the time of the second (and last) event in the Norg UGS.

3.2 Experimental results

De Kloe et al. (2008) conducted several uniaxial multi-cycle experiments on Norg-5 core samples with the objective to investigate possible fatigue mechanisms with continued loading and unloading. In these experiments, the pore pressure was cycled with radial stress being adapted to maintain uniaxial conditions:

- three times from 33 MPa down to 20 MPa and back,
- then 70 times from 33 MPa to 10 MPa and
- then three time from 33 MPa to 0.3 MPa.

The first three loading cycles between 33 and 20 MPa (330 and 200 bar) correspond most closely with the operating pressure in the Norg UGS. The three cycling ranges are recognized in the results of two experiments shown in Figure 9 and Figure 10.

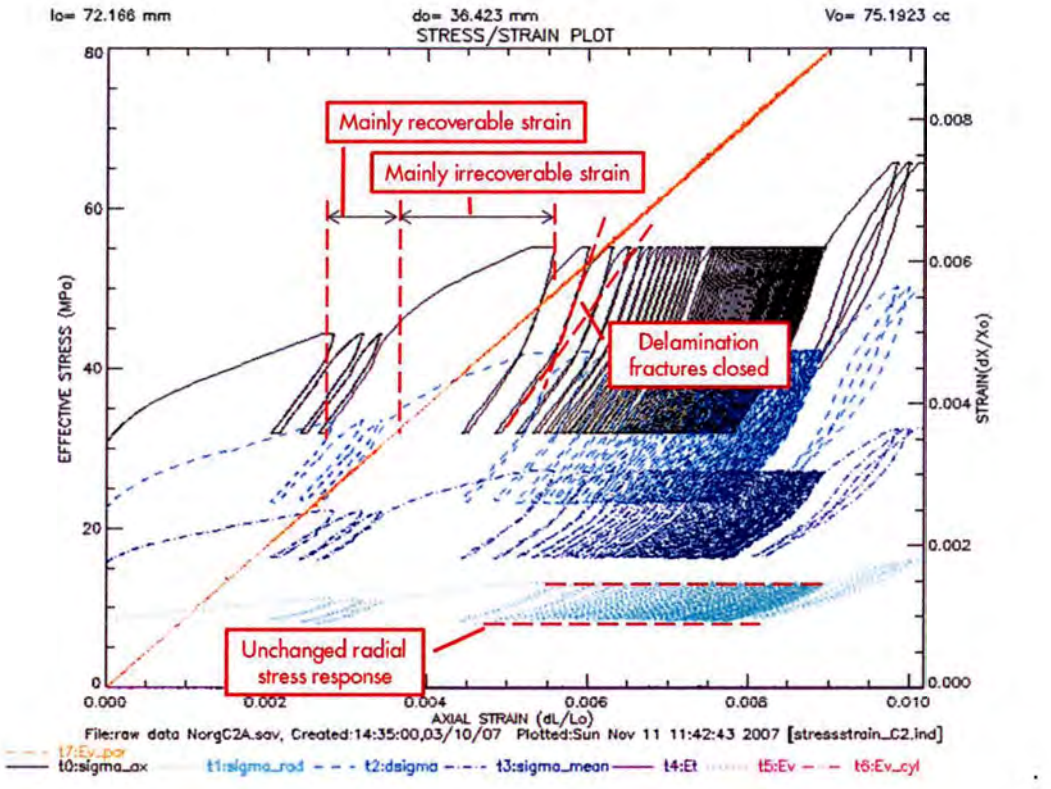

Figure 9 Effective vertical stress (black) and effective radial stress (light blue) as a function of axial strain over more than 70 loading and unloading cycles for Sample C-02

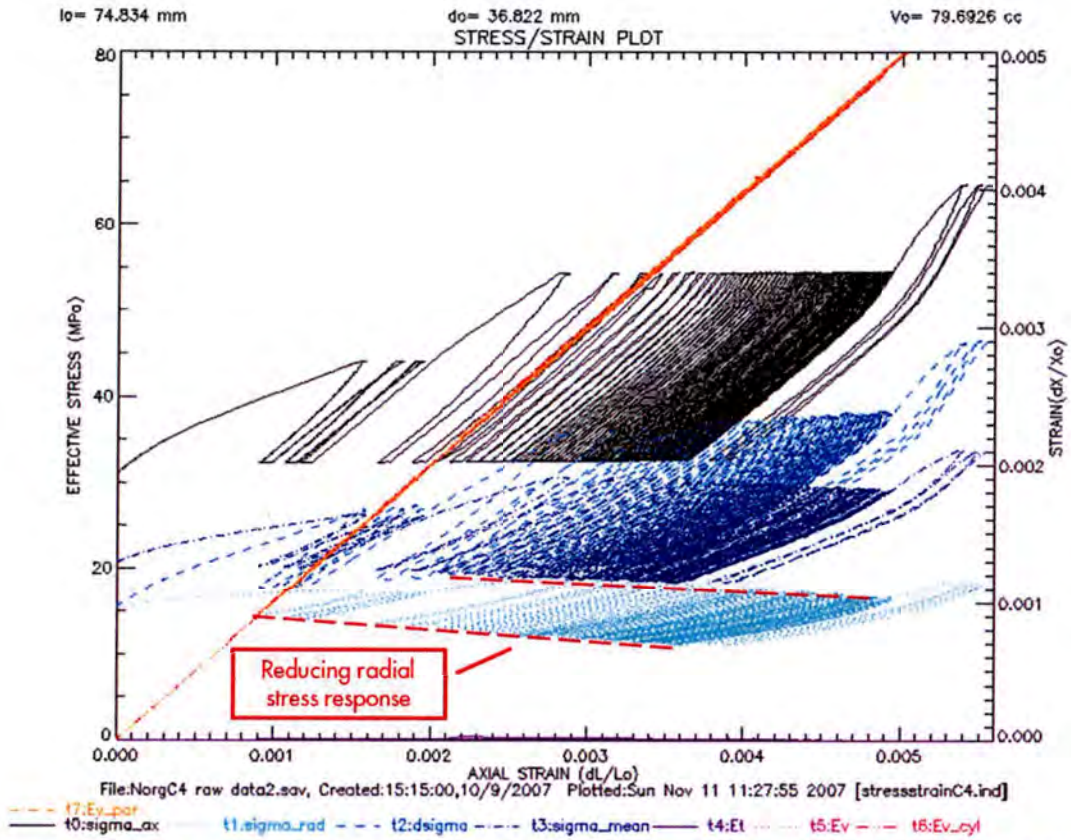

Figure 10 Effective vertical stress (black) and effective radial stress (light blue) as a function of axial strain over more than 70 loading and unloading cycles for Sample C-04.

The following observations can be made from the experimental results (Figure 9):

- Irrecoverable axial strain is accumulated in each loading cycle, in particular when increasing the effective stress beyond the previous maximum. The incremental axial strain is becoming smaller with every cycle between 33 and 10 MPa pore pressure. After a large number of cycles, the largest part of the incremental strain seems to develop when the effective axial stress is low (pore pressure is high) and constant for a while.
- Closure of horizontal delamination fractures in the samples are assumed by the Kloe et al. to be responsible for increasing stiffness (slope) in the loading and unloading branch during every cycle. The repeated opening and closure of these fracture does not seem to contribute to the accumulation of irrecoverable axial strain. The first three cycles between 33 and 20 MPa pore pressure do not show this kink very clearly, maybe because fracture closure is not fully achieved within this effective stress range. Delamination fractures may result from the core unloading process while bringing it to the surface and may not be present in-situ.
- The radial stress required to maintain uniaxial strain conditions remains fairly constant after every loading and unloading cycle. However, one experiment (Figure 10) showed a gradually reducing radial support stress, which implies that the deviatoric stress (Mohr-circle) is increasing.

The average Young's modulus in the 2nd and 3rd loading cycle from the five samples of Norg-5 well, given in Table 3, is 12840 MPa and the average Poisson's ratio is 0.186. This corresponds to a uniaxial compressibility of 15.6 10^{-5} MPa^{-1}. Elastic parameters from the first loading cycle are often influenced by microstructural rearrangements or damage incurred by the coring process. The elastic parameters from the second and third loading cycle usually provide better correlation with field observations.

The average Young's modulus from the five samples increases by 15% during the 2nd and 3rd unloading cycle (compared to the 2nd and 3rd loading cycle), while Poisson's ratio increases by 4%.

Table 3 Young's modulus and Poisson's ratio derived from pore pressure cycles between 33 and 20 MPa for the five Norg-5 samples (de Kloe et al, 2008).

	Sample C-01B		Sample-02		Sample-03		Sample C-04		Sample C-05	
	E [MPa]	Nu [-]	E [MPa]	Nu [-]	E [MPa]	Nu [-]	E [MPa]	Nu [-]	E [MPa]	Nu [-]
1st load	7420	0.15	4430	0.18	11400	0.15	7860	0.14	8150	0.10
1st unload	14200	0.17	14000	0.17	17700	0.25	16100	0.20	11400	0.13
2nd-3rd load	12900	0.16	11500	0.18	14900	0.25	12900	0.19	12000	0.15
2nd-3rd unload	15500	0.17	13800	0.19	16800	0.25	14600	0.20	13800	0.16

3.3 Stress

3.3.1 Vertical stress

The value of the vertical stress is dependent on the depth and thickness variation of the lithostratigraphic units. The impact of this variation on the stress gradients has been assessed by Zheng and Guises (2013) for the Groningen where the obtained range varied between 2.15 and 2.3 bar/10m. There are no wells available in Norg with a full coverage of density data but because of a similar geological setting we assume that this fairly narrow range is also valid for Norg. Using the density information that is presented by Nagelhout and Roest we conclude a value of 2.16 bar/10m at the top of the reservoir to be used as the recommended value for Norg.

3.3.2 Minimum horizontal stress Sh

A leak-off test in the Norg NRD-1 well (Figure 12) executed below the 7"shoe but exposed to the full open section that comprises ZE and ROCL and ROSL formations showed however a very high value for the leak-off pressure and this value was taken into account in later assessments of the fracture pressure for the Norg infill wells that were drilled in 2014. The value for the LOP is 2.1 bar/10m and conservatively we assumed in our assessments that this value represents the upper bound of the fracture pressure or fracture breakdown pressure. A hoop stress based back calculation was performed to retrieve the value of the Sh showing a value of 459 bar or 1.63 bar/10m. RFT measurements executed just after drilling the well measured however a depletion of 90 bar in the reservoir and therefore the value of the minimum stress needs to be corrected for this effect to obtain the ambient value for the minimum stress. Based on minifrac measurements in the northern part of the Netherlands, the current best estimate for the depletion constant is 0.62 (Figure 11).

Correcting the Sh for the depletion effect result in an estimated $Sh_{,ambient}$ value of 1.83 bar/10m. This value should be considered as the most likely value for the $Sh_{ambient}$ in Norg. This implies a K_{0min} value of 0.85.

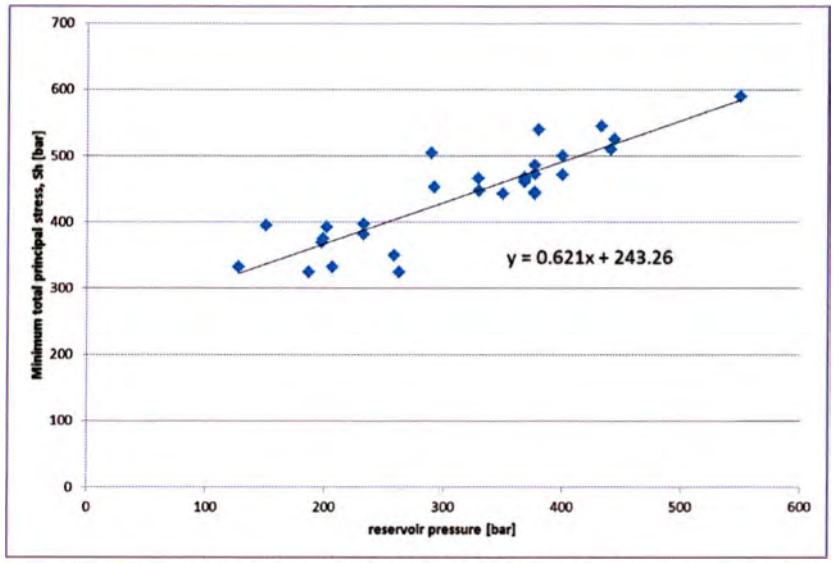

Figure 11 Fracture closure pressures from minifrac tests (y-axis) versus measured pore pressure in Rotliegendes formations in the northern part of the Netherlands.

3.3.3 Maximum horizontal stress or SH

There are no measurements available that could give an indication of the value of the intermediate principal stress or maximum horizontal stress in the Norg field. To provide an expected value for the SH we rely here on the measurements that are available for the Groningen field coming from various sources like logs and cores. These indicate a small difference between the two horizontal components between 5 and 10% (van Eijs, 2015). Therefore it is suggested to use 1.92 bar/10m as an expected value. This implies a K_{0max} value of 0.89.

3.3.4 Stress direction in Norg

The world stress map shows a direction of 171° East of North for the maximum horizontal stress in the Norg field (Figure 12). This value should be considered as the expected value for the Norg field.

3.4 Observations from subsidence data

The northern part of the Netherlands is monitored for surface movement with a high spatial and temporal frequency using a variety of techniques like optical sprit levelling, continuous GPS and InSar. These measurements were used to calibrate geomechanical models that then could be used for forecasting future subsidence in this sensitive area. Moreover these data could be used to investigate the hypothesis that some part of the compaction is irreversible, as also concluded from the core experiments. Figure 12 shows the result of a subsidence model that is fitted to all benchmarks in the area and compared in this figure to one benchmark in block 2. The production phase in the field leads to a subsidence of around 5.5 cm in this specific point. Figure 8 demonstrates that while the pressures during the first injection phase were brought to the ambient pore pressure, the subsidence was only partially reversed.

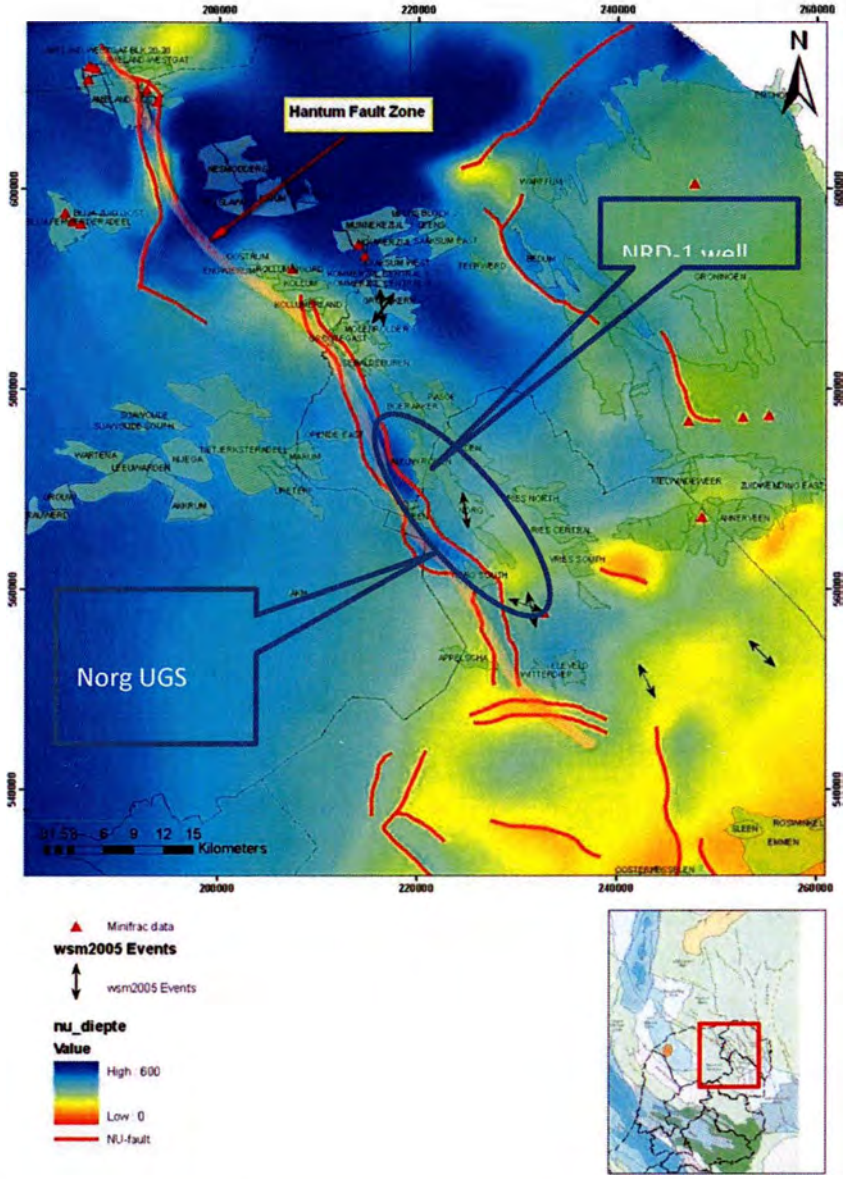

Figure 12 compilation of Neotectonic geological information (source: NAM, TNO). WSM2005 events indicate the stress direction of the maximum horizontal stress as available from the World Stress Map database. The contour map shows the thickness of the youngest deposits in the Netherlands. The thickness is influenced in some areas by recent fault movement.

A best fit was found when the reservoir stiffness was increased by a factor 2. This observation matches the observations from the core experiments (Table 3). Figure 14 shows the continuous measurement of a GPS antenna placed above the field over 2 years. The measurements clearly follow the decrease and increase of the pressure during two cylcles. The reservoir shows an elastic behaviour during these cycles also in line with the conclusions from the lab experiments.

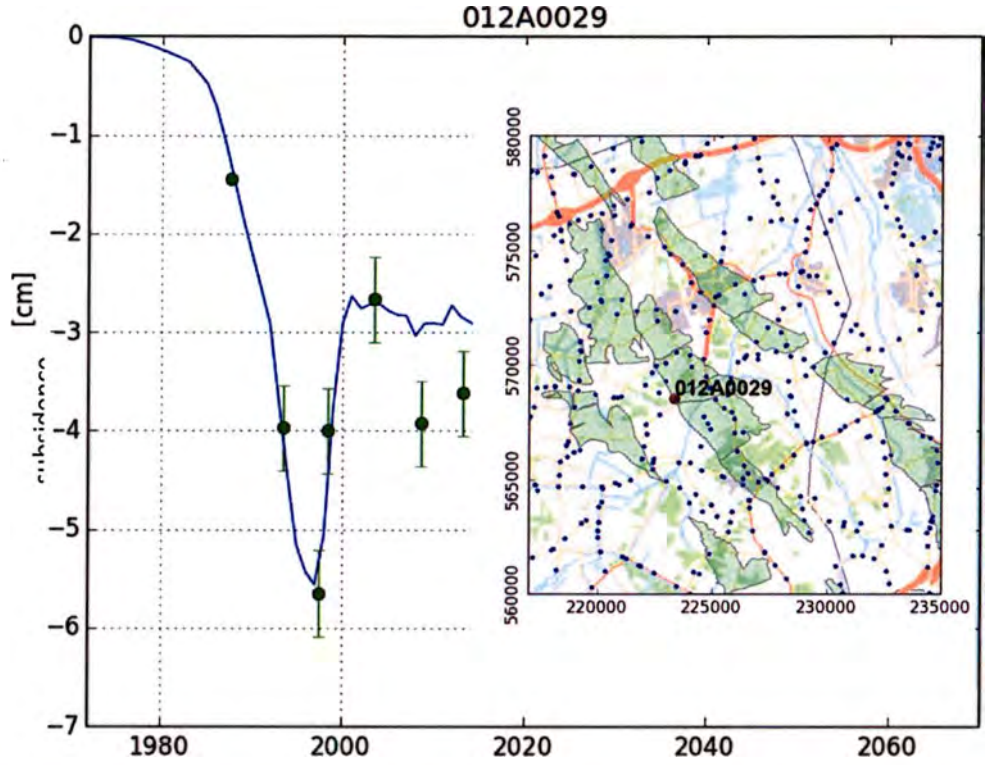

Figure 13 Comparison of measured subsidence (green dots + error bars indicating 2 SD uncertainty) and modelled subsidence (blue line). For and optimal match the stiffness was doubled during the first injection phase and subsequent production and injection cycles.

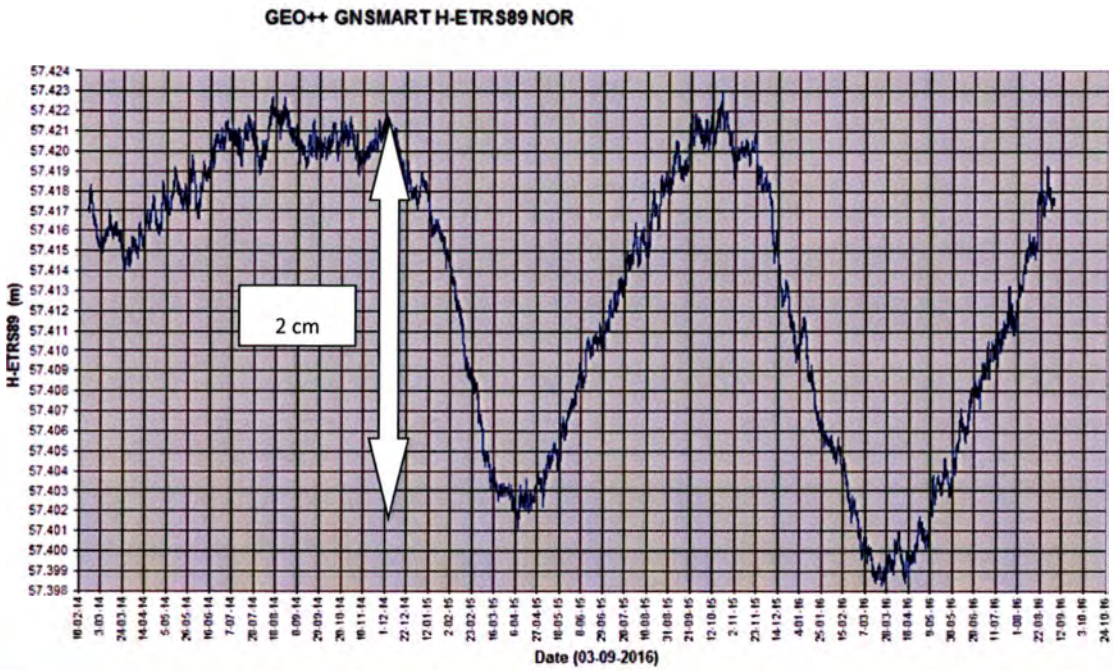

Figure 14 Vertical movement measured by continuous GPS above the Norg field as a result from production and injection cycles

4 General geomechanical considerations

Two general geomechanical concepts are taken into for the Norg storage plan, i.e. the effect of the loading rate and the memory or Kaiser effect that many (geo)materials show under cyclic loading conditions. These concepts are discussed in the next two sections.

4.1 The effect of loading rate during depletion

In addition to stress, the structure of the field and absolute pressure drop, production and injection rate may play a role in the in the induction of earthquakes. For the Groningen field research is currently taking place to investigate statistical and physical correlations between production rate and induced earthquakes. For Norg it can be observed that the only production-related seismic event occurred at a relatively low production rate. No more seismic events have been observed in the subsequent 17 years, despite the fact that the production rate has been much larger in subsequent years (Figure 15). From this observation we conclude that the production rate does not appear to have a significant effect on seismic activity rate in Norg.

4.2 Kaiser effect

The Kaiser effect occurs during measurements of acoustic emissions in rock mechanical experiments but is also observed with micro seismic monitoring during hydraulic fracturing jobs in the subsurface. Typically in these cases the number/rate of seismic or acoustic signals only increases when loading of the specimen or subsurface exceeds a previously applied stress level. The rock thus exhibits a stress memory effect.
In our case, the UGS Norg "memorizes" a maximum loading level of the rock in block 2 at pore pressure of 190 bar. New earthquakes could occur, according to the Kaiser effect, when the pressure will drop to a level beyond the 190 bar. Analogue fields neighbouring the Norg UGS did already experience larger pressure drops without showing a high seismic activity rate but prudency is recommended because loading rates were much smaller in these fields.

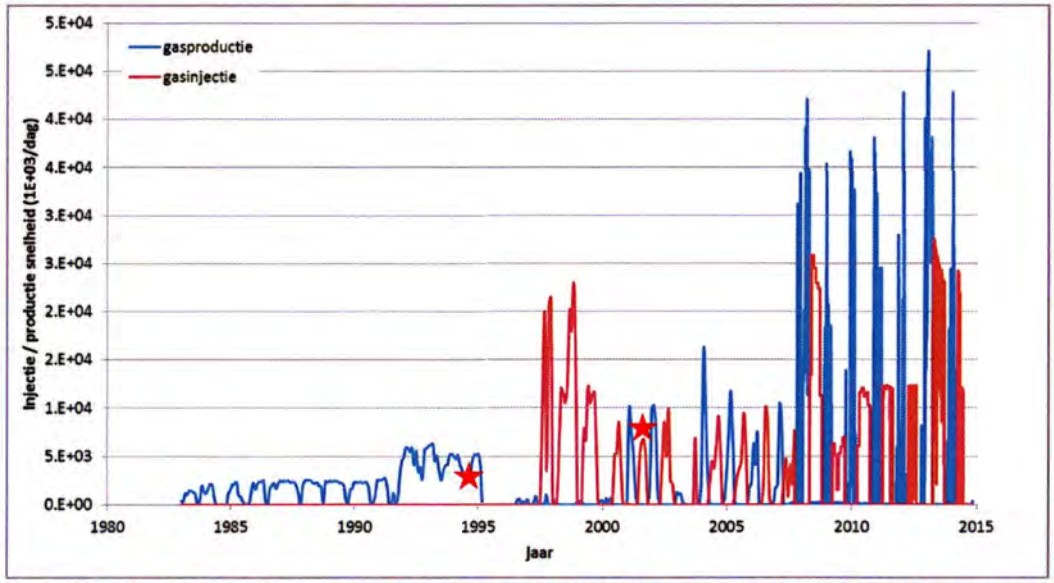

Figure 15 Measured injection and production rates in the Norg UGS. The two red stars indicate the moment that the earthquakes happened.

4.3 Modelling strategy

The main physical processes that could lead to induced seismicity are documented in e.g. TNO (2016 a,b,c):

- An increase in the pressure in the fault zone relative to the pressure in the rock. A relative increase in pressure in the fault zone leads to a decrease of the normal stress on the fault plane. This reduces the shear strength of the fault without reducing the actual shear stress, and could therefore lead to fault slip. This mechanism occurs especially when faults have a higher permeability compared to the surrounding rock. The permeability in the Norg UGS reservoir rock is very high and therefore it is expected that this mechanism is not important.
- A temperature difference between the injected gas and the rock mass. This may lead to additional shear stress around injection wells and therefore poses a threat for fault stability. The injected gas in Norg has a temperature between 90 and 95 degrees Celsius, which is close to the ambient temperature of the field. Therefore, significant temperature-induced stress changes are unlikely in the Norg UGS.
- Irreversible stress paths. Stress paths during the first stages of production and injection are generally not reversible. This can be caused by non-elastic (plastic) deformation of the rock and fault slip during the initial depletion stage. In the following injection stage, the rock will unload following an elastic stress path. This is observed in experiments conducted on Norg UGS core material (Section 3.2). Results from numerical models that are described by TNO (2016c) have shown that in some scenarios irreversible stress changes can increase the seismic threat. This mechanism is perceived most relevant for the Norg UGS and evaluated in detail in subsequent sections.

For Norg this effect could occur after the first injection cycle, but in the following cycles, the stress paths will mainly proceed in a reversible way until the pressure becomes lower than the lowest pressure that is seen during the operating history of the field (190 bar) or higher than the highest pressure (347 bar).
It can be concluded that the lack of observed seismicity over the last 17 years can be explained by the above considerations. It should be stated that these considerations are only qualitative knowing that no predictive model exists for induced seismicity, especially in a case like Norg where the number of tremors is too low in order to calibrate models or mechanisms to validate statistically. Earthquakes cannot be ruled out in the future and therefore it is recommended to expand the seismic monitoring network around Norg so that smaller earthquakes can be observed. Knowledge about the small tremors often leads to an increase in our understanding of possible larger earthquakes. Expansion of the network has already taken place and three additional geophone stations are operational since early 2016.

5 Modelling of possible fault reactivation

5.1 Approach

Objective is to investigate the relationship between reservoir pressure and fault stability under gas production and storage conditions. Special attention is paid to potential changes in the stress path that could impact the upper and lower limits of the allowable reservoir pressure. An approach with 2D cross sections is chosen as both structure and stress directions allow for a plane strain approximation. This approach is in analogy to Nagelhout & Roest (1997). Recently it has been shown

(van den Bogert, 2015) that the zone of stress disturbance around a fault that intersects a depleting reservoir is limited to one or two times the reservoir thickness. For the Norg UGS this implies that stability of faults further away than 150-300 m can be treated as independent cases as far as the onset of fault slip is concerned. Furthermore, the absence of multiple seismic events within a short time frame also suggests that a seismic event on one fault does not trigger events on other faults. For these reasons, the potential stress-path dependency of the allowable reservoir pressure limits is assessed using two-dimensional cross sections.

Two cross-sections perpendicular to two faults have been used to develop potential hypotheses for earthquakes under production and storage conditions. These two cross- sections have been taken from the sixteen cross sections generated across the Norg UGS (Figure 16 and Enclosure-1). One cross section (number 7, Figure 17) is taken at the location of the Langelo event on 5 March 1993 (M_l=1.5) and the second (cross-section 16, Figure 18) is taken at the location of the Steenbergen event on 7 June 1999 (M_l=1.1). The cross sections incorporate the correct depth, formation thickness and offset, as well as the fault orientation at the seismic event locations. These geometrical aspects have a large impact on the fault slip behaviour (van den Bogert, 2015). The hypotheses formulated in this chapter are described in terms of fault slip parameters that can simulate onset of instable, seismic slip along the fault plane of cross section 1 at about 225 bar reservoir pressure during the initial production stage of the field and along the fault plane of cross section 2 at about 325 bar reservoir pressure during the first storage cycle.

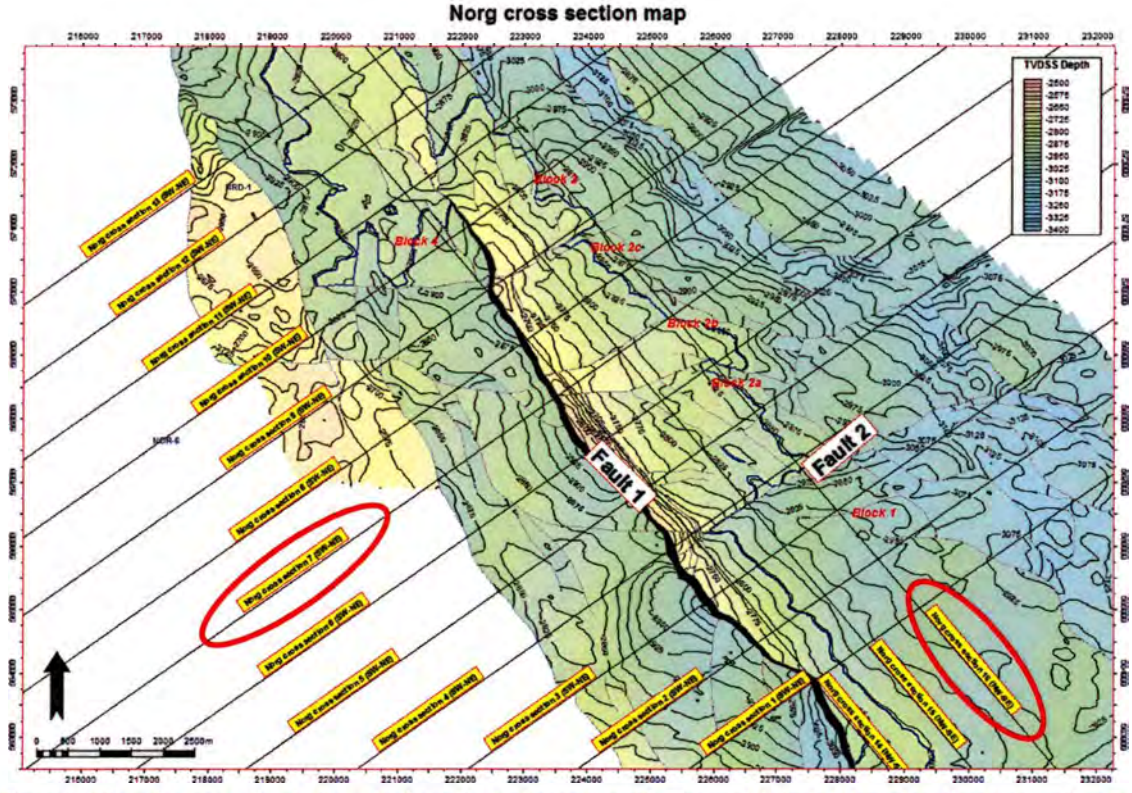

Figure 16 Map of cross section that can be found in enclosure 1 and 2. The model study is based on the cross section 7 and 16 indicated by the red ellipses

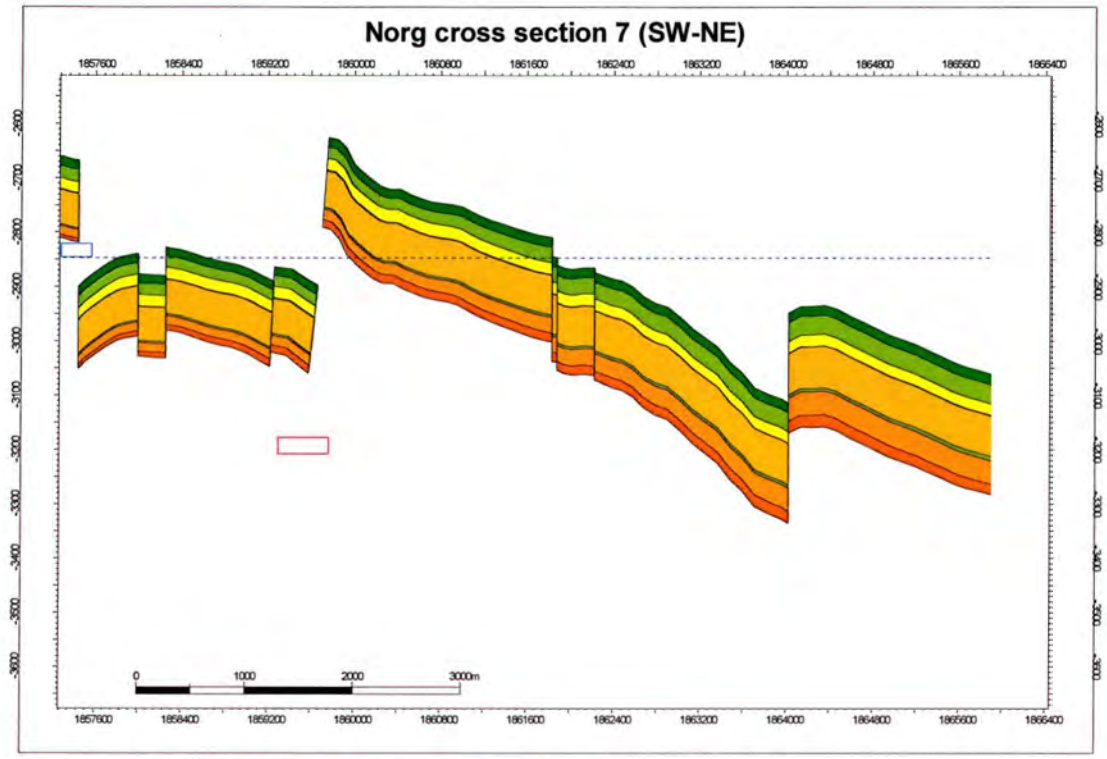

Figure 17 Cross section 7 showing the large offset over fault 1

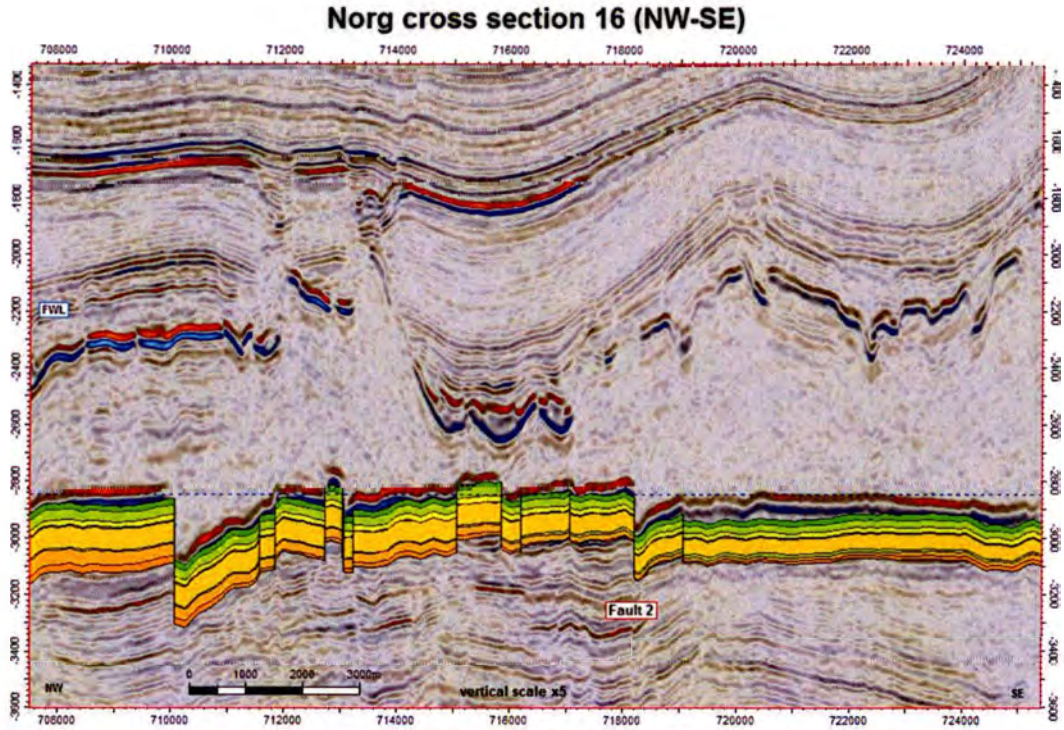

Figure 18 cross section 16 (NW-SE) perpendicular to fault 2 showing a much smaller offset over this fault

A qualitative assessment is made for the stability of other fault locations in the Norg UGS based on the two hypotheses for the seismic events. Thereby it is considered that the fault stability condition has been most critical in these two locations.

The two-dimensional model is described in section 5.2, followed by the stability assessment of cross section 1 in section 5.3. In this section, it is explained that fault slip is not the same as seismic rupture. The essential conditions for onset of seismic rupture are described and implemented in the hypothesis for cross section 1. The consequences of some of the modelling assumptions are discussed for cross-section 1 but can be applied as well to cross-section 2.

5.2 Model

Formation layering and thickness for the two cross sections is taken from Nagelhout en Roest (1997, Table 2 in Chapter 3) and is summarised in Table 4. The overburden in the model includes Tertiary Upper, Middle and Lower North Sea groups , the Cretaceous Chalk and Rijnland groups, and the Triassic Upper and Lower Germanic Groups. Total thickness of these formations is set to 2240 m in the model. The Zechstein rock salt thickness above the Norg field is set to an average value of 290 m (varying between 230 and 400 m), and the Ten Boer Claystone is set to 70 m thickness. Reservoir thickness, which includes Lower Ten Boer and non-conglomeratic Slochteren formations, varies between 130 and 150m. An average thickness of 140m is assumed in the model, divided over 3 depleting reservoir units. The Limburg group is the model basement down to 6000m TVD.

Table 4 Norg Stratigraphy assumed for the two cross-section models

Model layer	Geology	TVDNAP Top (m)	Thickness (m)	Depletion
Overburden	U., M. & L North Sea, Chalk, Rijnland, U. & L. Germanic	0	2240	
Layer 1	Zechstein Rock salt	2240	290	
Layer 2	Zechstein Ten Boer	2530	70	
Layer 3	U. Rotliegend	2600	50	Yes
Layer 4	U. Rotliegend	2650	40	Yes
Layer 5	U. Rotliegend	2690	50	Yes
Basement	Limburg	2740	3260	

Formations are assumed to behave linear-elastically. Young's modulus and Poisson's ratio for all formations excluding the reservoir properties are taken from Nagelhout and Roest (Table 5) to simulate the initial depletion stage of the field. The uniaxial compressibility of the reservoir (layer 3, 4 & 5 in Table 5) is 15.7 10^{-5} MPa^{-1}, and is the same as the uniaxial compressibility derived from the 2nd and 3rd loading cycle in the experiments by de Kloe et al. (Table 3). The Zechstein Rock salt has been assigned a Poisson's ratio close to 0.5 to capture the nearly incompressible and isostatic stress behaviour.

Formation density is taken from Nagelhout and Roest (1997) in order to arrive at a realistic total vertical stress as a function of depth (table above), while the horizontal components were mainly derived from the NRD-1 leak-off test (chapter 3). The minimum total horizontal stress ratio is k_{0min} = 0.85 and the maximum total horizontal stress ratio k_{0max} = 0.89.

Table 5 Density and linear-elastic formation properties assumed for each formation layer

Model layer	Thickness (m)	TVDNAP Top (m)	Density (kg/m3)	Young's modulus	Poisson's ratio
Overburden	2240	0	2230	17.5	0.224
Layer 1	290	2240	2100	31.0	0.499
Layer 2	70	2530	2900	51.8	0.295
Layer 3	50	2600	2400	14.7	0.227
Layer 4	40	2650	2400	14.7	0.227
Layer 5	50	2690	2400	14.7	0.227
Basement	3260	2740	2650	40.6	0.193

A material point on the fault plane will start slipping if the local shear stress τ is equal to the local shear strength τ_{max}, which is defined by a Mohr-Couloumb frictional slip criterion (Figure 19):

$$\tau_{max} = C + \sigma_n \tan \varphi$$

Herein, C is the cohesion stress, φ is the angle of internal friction, and σ_n is the normal effective stress in the material point on the fault plane. In this report the (initial) friction coefficient μ_i=tan φ is used to define the shear failure envelope. Furthermore, the Shear Capacity Utilisation SCU is used to express the onset of fault slip, which is defined as

$$SCU = \frac{\tau}{\tau_{max}}$$

The material point on the fault behaves linear-elastically if SCU < 1. Inelastic slip displacement along the fault interface is accumulated if SCU=1, whereas a value larger than 1 is not possible. Furthermore, it is assumed that the initial friction coefficient μ_i at the onset of fault slip reduces to a residual friction coefficient μ_r if the relative slip displacement D across the fault plane reaches the critical value D_c. (see right-hand side of Figure 19), which represents a slip-weakening mechanism. In this report a linear fault slip-weakening relationship is assumed. Furthermore, the fault slip model incorporates a so-called dilatancy angle ψ, which expresses the ratio of the normal over the slip displacement after the onset of slip.

Unfortunately, no experimental data is available to constrain the fault slip properties for the Norg UGS. In this study the fault slip properties are adjusted such that the observed seismic events are simulated by the 2D fault slip model. As point of departure, a cohesion stress of 10 MPa is assumed and the initial friction coefficient of μ_i is set to 0.6 (φ=30.96°). This allows a linear-elastic assessment of the fault structure and gains insight how fault slip changes the simulated response of the subsurface for more realistic values of the fault properties. The dilatancy angle ψ is 0° for all simulation in this study.

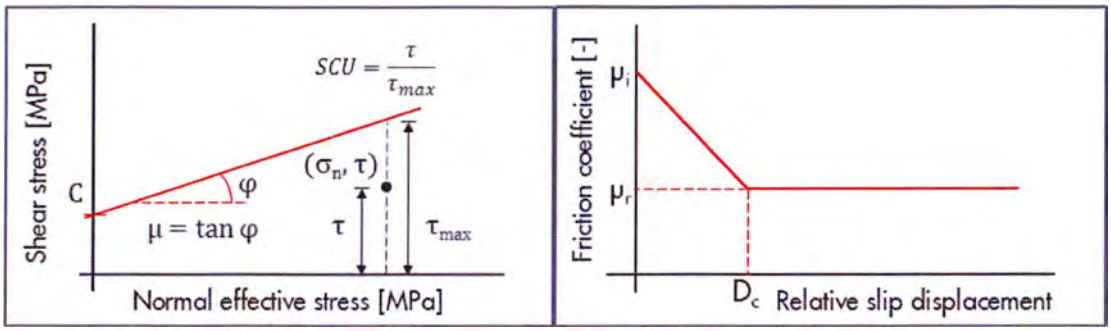

Figure 19 Left: Mohr-Coulomb shear failure criterion, specified by Cohesion stress C and friction angle φ. Right: Linear slip-weakening relationship assumes a reducing fault friction coefficient with increasing (relative) slip displacement.

Table 6 Fault properties

Model layer	Cohesion C [MPa]	Initial friction μ_i [-]	Residual friction μ_r [-]	Critical slip displacement D_c [m]
Overburden	10	0.6	0.3	0.02
Reservoir	10	0.6	0.3	0.02
Basement	10	0.6	0.3	0.02

A hydrostatic pore pressure gradient (10 kPa/m) is taken for the overburden above the rock salt and in the Ten Boer Members. The (gas) density gradient in the reservoir is 1.8 kPa/m with a Gas-Water Contact (GWC) at 2740 m depth and 32.7 MPa (327 bar). This GWC coincides with the bottom of the Rotliegend reservoir. The saline water gradient below the reservoir is assumed 11.66 kPa/m. Finally, reservoir depletion pressure and subsequent re-pressurisation is simulated by a step-wise reduction and increase of the pore pressure in the 140 m Rotliegend reservoir. The pressure in the fault follows the pressure in the adjacent formation. So, the fault pressure changes only over the interval that is exposed to a depleting reservoir. This is based on the assumption that lateral fault permeability is good. The exact reservoir pressure scenario is described for each cross-section.

5.3 Geomechanical analysis of the first seismic event

In this section, a model hypothesis is formulated that could explain the first seismic event on 5 March 1993 during the initial production stage of the Norg field at a reservoir pressure of 225 bar. This seismic event has been mapped on to the main NW-SE bounding fault, Fault 1 (F1), in cross section 7 (Enclosure-1). Fault 1 is making an angle of 66 degree with the vertical axis, off-setting the Slochteren Formation by 360 m, and is assumed to be oriented perpendicular to the minimum horizontal stress. Further structural detail is provided in Figure 20.

The right-hand graph in Figure 20 shows the interval where the pore pressure has been reduced from 32.7 to 17.7 MPa (327 to 177 bar) simulating the initial production stage of the field. The green bars indicate the Rotliegend interval in the depleting foot wall and the non-depleting hanging wall. The salt intervals in the foot- and hanging wall are indicated by the grey bars. The virgin pore pressure (blue line) is as specified in Section 5.2, whereas the red line reflects to depletion of 15 MPa.

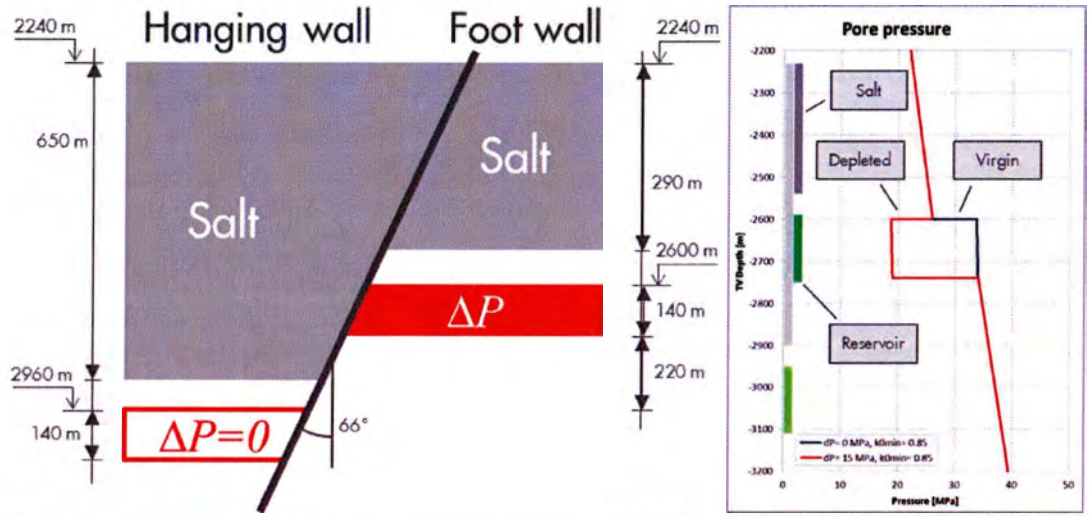

Figure 20 Left: Simplified cross section used for the stability analysis of Fault F1. The Slochteren Formation is indicated in red, while the overlying non-depleting Ten Boer Member is white. Right the pore pressure distribution along the fault plane as a function of depth under virgin and depletion conditions.

Figure 21 shows the finite-element mesh used to simulate the response of Fault 1 to reservoir depletion. 280 Interface elements with a length of 0.5 m are used to accurately capture the slip displacement and (peak) stress distribution along the fault plane. A small element size is required to achieve convergence of the numerical simulation for brittle failure of the fault when the critical slip displacement D_c is small (Buijze et al., 2015). This small element size is selected so that the same mesh could be used for all analyses, while preventing numerically induced artefacts.

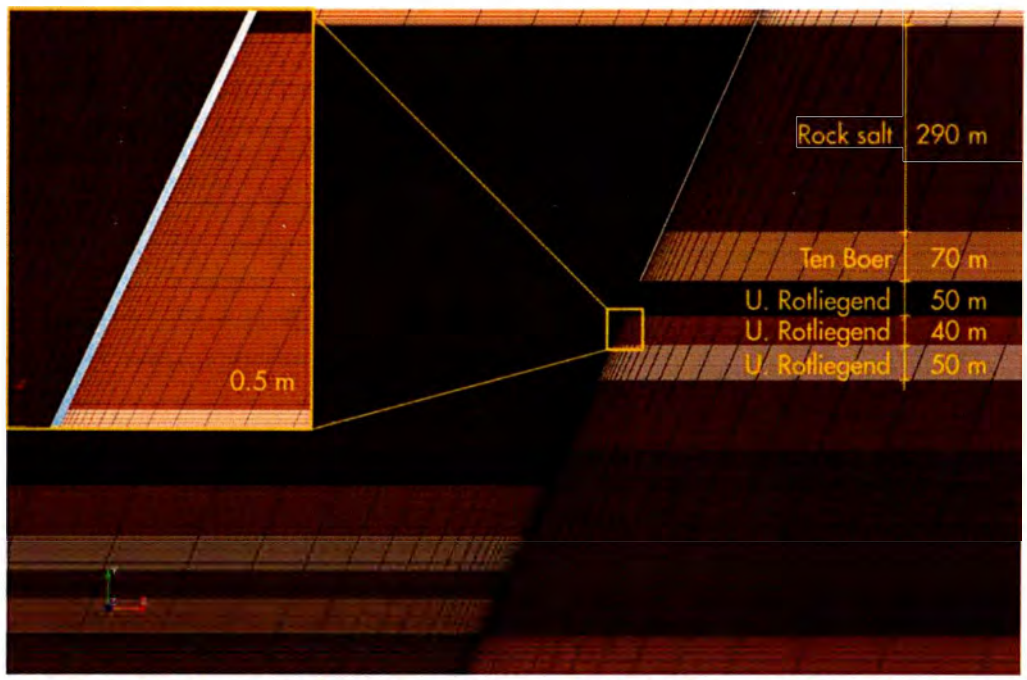

Figure 21 Finite-Element mesh for Cross-section 1, with 140 m depleting Upper Slochteren Member in the foot wall (right-hand side of the fault), overlain by 70 m Ten Boer Claystone and 290 m Rock salt. There is no depletion in the hanging wall, left of the 65 degree dipping fault, which is offset by 360 m relative to the foot wall. This is accommodated by a rock salt thickness of 650 m.

Pressure depletion is simulated in the foot wall reservoir unit, while pore pressure is kept constant in the Slochteren Formation in the hanging wall (Figure 20). Reservoir block 2 pressure is reduced in a step-wise fashion starting at a virgin pressure of 32.7 MPa (327 bar) down to 17.7 MPa (177 bar), which is about the minimum average pressure measured in block 2. This is equal to a depletion of 15 MPa (150 bar). The seismic event that occurred at about 225 bar equates to a reservoir depletion pressure of about 10 MPa (100 bar).

Complexity of the model approach is increased in the next three sections. First, in section 5.3.1, a high value for the fault cohesion and friction angle is taken to suppress any fault slip and facilitate the assessment the potential critical location along the fault plane. Subsequently, in section 5.3.2, the impact of a lower minimum horizontal stress through the value for k_{0min} is evaluated. Last, in section 0, the fault slip parameters are adjusted to simulate onset of seismic rupture (Table 7). The parameters varied in the first two sections are summarised in Table 8 All other modelling assumptions are in accordance with section 5.2.

Table 7 Overview of stress ratio used in the various cases.

Case	K_{0min} [-]	K_{0max} [-]	Comment
F1-1	0.85	0.89	For all formations
F1-2	0.95	0.99	$K_{0min}=k_{0max}=1.0$ for salt
F1-3	0.85	0.89	$K_{0min}=k_{0max}=1.0$ for salt, Section 5.3.1, base case
F1-4	0.80	0.84	$K_{0min}=k_{0max}=1.0$ for salt
F1-5	0.75	0.79	$K_{0min}=k_{0max}=1.0$ for salt
F1-6	0.70	0.74	$K_{0min}=k_{0max}=1.0$ for salt
F1-7	0.65	0.69	$K_{0min}=k_{0max}=1.0$ for salt

5.3.1 Linear-elastic response

Figure 22 shows the results of 15 MPa (150 bar) reservoir depletion from 327 bar to 177 bar when onset of fault slip is suppressed by assuming high values for cohesion and friction coefficient (Analysis F1-3).

The virgin (effective) normal stress distribution along the fault plane (blue line, left graph in Figure 22) shows various discontinuities that are the result of the assumptions made. The shallowest discontinuity reflects the difference of the minimum horizontal stress in the overburden ($k_{0min}=0.85$) above 2240 m and in the salt ($k_{0min}=1$). The second discontinuity at 2530 m depth is caused by the juxtaposition of salt in the hanging wall against the Rotliegendes Ten Boer Member in the foot wall. The third discontinuity at the top of the block 2 reservoir at 2600 m depth is caused by the assumption of the over pressure caused by the gas cap. The jump to a higher pore pressure from Ten Boer to Slochteren Formation (top-left graph) causes a lower normal effective stress on the fault plane. The fourth and last discontinuity at the bottom of the rock salt in the hanging wall at 2890 m depth is again caused by the different horizontal stress ratio in the salt (1.0) and the basement (0.85).

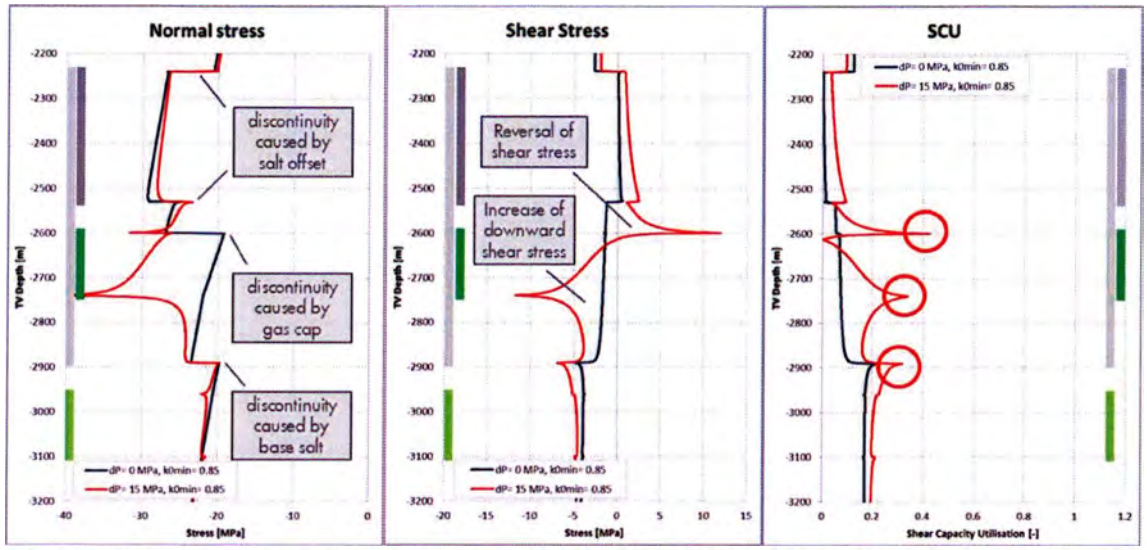

Figure 22 Normal (effective) stress, shear stress and Shear Capacity Utilisation (SCU) as a function of depth along the fault plane, under virgin reservoir conditions (blue line) and under 15 MPa (150 bar) depletion.

The normal stress along the fault plane predominantly increases over the depleting reservoir interval (red line, compressive stress is negative in this report). The fault normal stress also increases also below the foot wall reservoir, but to a lesser extent. Above the foot wall reservoir, in the Ten Boer and Salt formations, the normal stress reduces somewhat in response to the depletion. This is important to note, because the capacity of the fault to carry shear stress is influenced by the normal stress acting on it according to the assumed Mohr-Coulomb friction law.

Reservoir depletion in the foot wall reservoir introduces two peaks in the shear stress distribution along the fault plane (middle graph in Figure 22). One at the top, and one at the bottom of the depleting formation. The initial shear stress distribution (blue line) reflect the isotropic stress condition in the salt formation where $k_{0min}=k_{0max}=1.0$, and shear stress level associated with $k_{0min}=0.85$ for the formations below the salt in the hanging wall. Negative values indicate shear stress in downward direction in this analysis, while positive values represent upward shear stress. It is seen that reservoir depletion causes an increase of (downward) shear stress at the bottom of the foot wall reservoir and incremental upward shear stress at the top of the reservoir causing a reversal shear stress direction. The two depletion-induced shear stress peaks are at the interface with non-depleting formations. Furthermore, it is seen that the fault shear stress induced by depletion is felt to up to a few hundred meters away from the reservoir in a diminished sense.

The Shear Capacity Utilisation (SCU) distribution shows three potential critical locations for fault slip: the two induced by depletion as discussed above, and one at the bottom of the salt in the hanging wall. The latter location is introduced by the initial stress assumptions and is aggravated by depletion. This peak in SCU value would not exist if a uniform horizontal stress condition would be assumed. The SCU peak at the top of the reservoir is reflecting the strong reversal of shear stress caused by the depletion, and indicates a potential for reversal slip. The two other peaks are associated with dip-slip events in downwards direction. The SCU peak values in Figure 22 remain well below 1, implying shear stress values below the local shear strength . This is due to the high value assumed for the cohesion (10 MPa)

5.3.2 Impact of minimum horizontal stress uncertainty

Six analyses have been conducted with different values for the horizontal stress ratio to demonstrate the impact of the minimum horizontal stress assumption on the potential slip locations (Table 7).

First, consider the virgin normal and shear stress distribution for analysis F1-1, represented by the red line in Figure 23. In this "thought experiment" salt is replaced by a formation that can hold shear stress, by assuming k_{0min}=0.85. The normal and shear distribution below the salt in the hanging wall from analysis F1-1 hides the results from analysis F1-3 (base case) discussed in the previous section. The discontinuity in the normal stress at the bottom of the hanging wall does not appear. Actually, the only discontinuity in the normal stress distribution that remains is caused by the over pressure that results from the gas cap at the top of the reservoir in block 2 at 2600 m depth. The fault normal stress is larger over the interval where it is exposed to salt. Also, the three discontinuities that show in the base case situation disappear in the ambient shear stress and SCU distribution (middle graph in Figure 23), only leaving a SCU discontinuity at the gas cap.

Cases F1-2 through F-7 have been evaluated to assess the impact of the uncertainty in the ambient minimum horizontal stress for all non-salt formations. In this series, the k_{0min} value is varied between 0.95 and 0.65. Compared to the base-case F1-3 discussed in the previous section, it is seen that a k_{0min} value closer to 1 reduces the absolute shear stress level and reduces the magnitude of the discontinuities introduced by the presence of salt. Inversely, a k_{0min} value lower than 0.85 would increase shear stress, SCU and magnitude of the discontinuities. In particular, the SCU below salt in the hanging wall is most sensitive to the k_{0min} value.

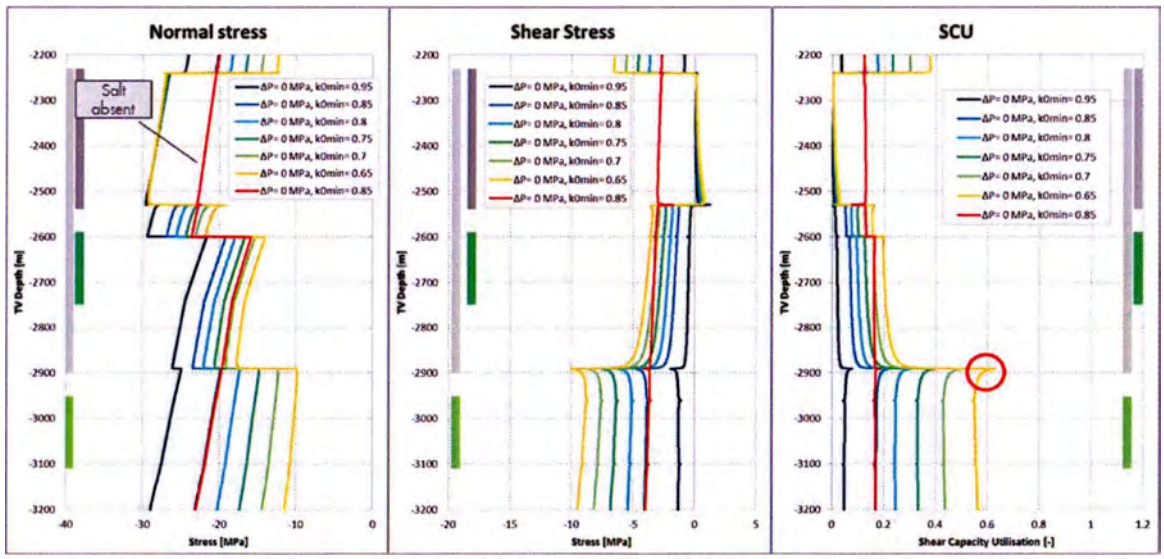

Figure 23 Normal stress, shear stress and Shear Capacity Utilisation (SCU) as a function of depth along the fault plane, under virgin reservoir conditions for different values of k_{0min}. The red line represent the case in which salt is absent and k_{0min}=0.85 would be assumed for all formation.

So, it is found that the presence of salt has a significant impact on the initial stress distribution, and thereby on the potential locations for fault slip. Salt-induced discontinuities in the fault normal stress distribution introduce locations with SCU peak values which may become nucleation points of fault slip and potentially seismic rupture, e.g. for Fault 1, such a location is found at the base of the salt at

2890 m depth. Furthermore, the potential critical locations at the top and particularly at the bottom of the depleting formation are less pronounced due to the presence of salt. The model suggests that the presence of salt enables other locations on the fault plane to become critical. For Fault 1, this location is at the bottom of the salt in the hanging wall.

5.3.3 Fault properties that simulate onset of seismic rupture

In this section, the fault properties are adjusted assuming the base case stress condition described in section 5.2, such that onset seismic rupture is simulated after 10 MPa (100 bar) reservoir depletion according to the principles shown in the right picture of Figure 19. After several iterations, five different sets of fault parameter are found as summarised in Table 8. First, cohesion is set to 0 MPa compared to 10 MPa for the cases discussed in the previous two sections. Subsequently, the initial friction coefficient has been reduced to simulate the onset of fault slip at a depletion level below 10 MPa. Finally, the critical slip displacement D_c has been reduced from 0.02 m to the values listed in the table to arrive at an instable fault condition at about 10 MPa reservoir depletion.

Figure 24 shows the development of the slip patch length as a function of reservoir depletion for the five cases in Table 8. Onset of non-seismic fault slip is recognised by a slip patch length larger than zero, which occurs at the bottom of the salt in the hanging wall (Figure 25). For a fault without cohesion, this occurs after less than 1 MPa reservoir depletion for a friction coefficient of 0.25 and after 6.4 MPa for a friction coefficient of 0.29. Smaller values for the friction coefficient than 0.25 would imply that the fault is critically stressed under virgin reservoir conditions, which is considered not realistic.

Onset of seismic rupture is recognised by the vertical slope of the slip-depletion curves in Figure 24. The vertical slope implies that no additional depletion is required to propagate the slip patch. This is caused by the slip weakening behaviour assumed for the fault as shown in Figure 19 (Buijze et al, 2015). Faults remains stable, and require additional depletion to propagate the slip patch if no slip weakening is assumed after the onset of fault slip (van den Bogert, 2015). It is a given by the used assumptions that the fault is in unstable equilibrium at the onset of seismic rupture.

The slope of the slip-weakening branch in Figure 19 (right-hand graph) determines the critical slip length required to bring the fault to a condition of instable equilibrium (Buijze, 2015). A smaller value for D_c causes a steeper slope in the slip-weakening relationship and causes instable equilibrium to occurs at a smaller length of the slip patch. This response is confirmed by Figure 24 and Figure 25. This also explains why a smaller value for D_c is required for a larger value of the initial friction coefficient in order to arrive at the same depletion level at which instability occurs.

Table 8 Overview of model properties used.

Case	Cohesion [MPa]	Initial friction coefficient μ_i [-]	Residual friction coefficient μ_r [-]	Critical slip displacement D_c [m]	Depletion at onset of fault slip [MPa]	Depletion at onset of seismic rupture [MPa]
F1-11	0	0.25	0.15	0.0050	<1.0	9.79
F1-12	0	0.26	0.16	0.0034	2.2	10.05
F1-13	0	0.27	0.17	0.0022	3.6	10.07
F1-14	0	0.28	0.18	0.0014	5.0	9.97

F1-15	0	0.29	0.19	0.0010	6.4	10.20

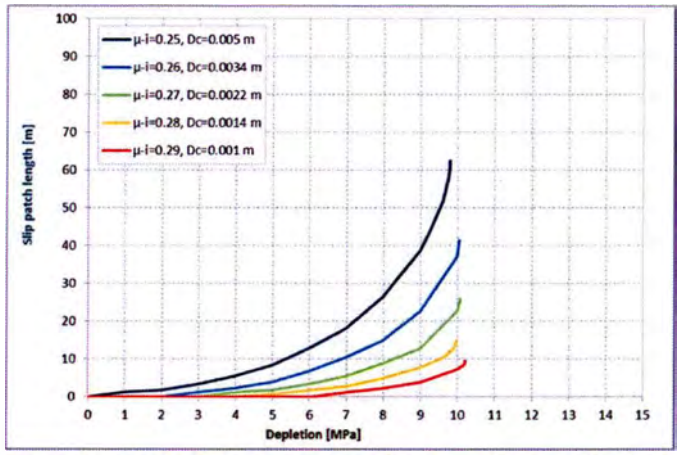

Figure 24 Length of the slip patch as a function of depletion for the five cases listed in Table 8. Five scenarios are shown that trigger an earthquake at around 10 MPa reservoir depletion.

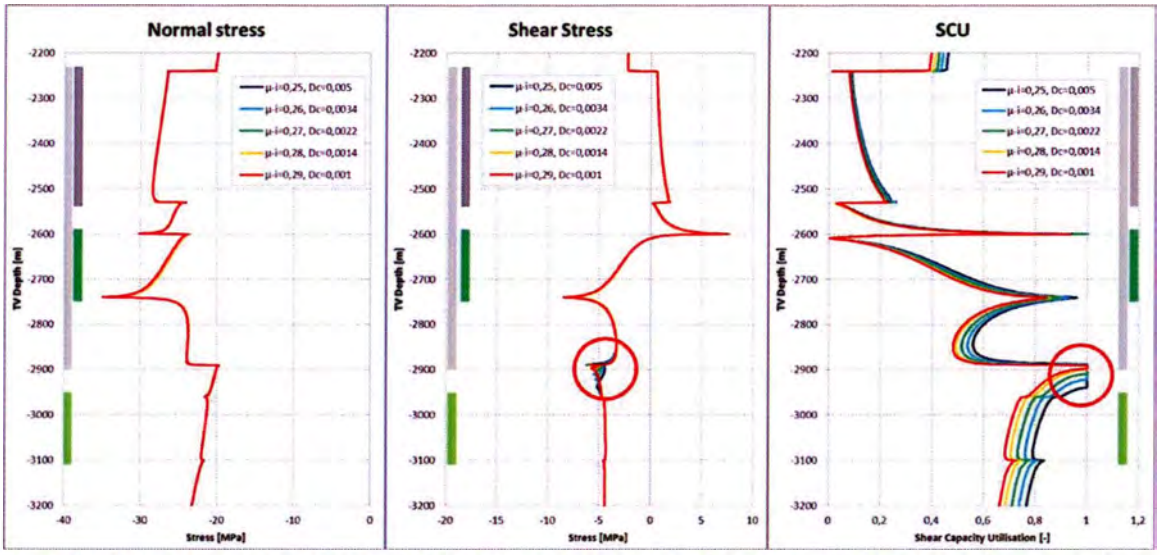

Figure 25 Normal stress, shear stress and Shear Capacity Utilisation as a function depth at the onset of seismic rupture (at about 10 MPa depletion). The red circle in the right-hand graph highlight the location and length of the slip patch. The red circle in the middle graph highlights the reduction of shear stress caused by the slip-weakening relationship.

5.4 Geomechanical analysis of the second seismic event

The second seismic event in the Norg UGS occurred on 7 June 1999 and is mapped on a Fault F2 separating block 1 and block 2 in cross section 16 (Enclosure-1). The objective is to formulate a hypothesis that could explain the seismic event after the first storage cycle in the Norg field. To this end, the stability of Fault F2 associated with this second seismic event is assessed by simulating an initial reservoir depletion of 15 MPa (150 bar depletion from 327 bar to 177 bar) followed by a re-pressurisation of 15 MPa, back to the original reservoir pressure.

For this purpose, a 2D geomechanical model (Figure 26) is used, including the Zechstein Rock salt at 2500 m TVD, 70 m of Ten Boer clay stone overlying the 140 m thick Upper Slochteren Member, which is offset by 130 m along Fault F2, which has a dip angle of 85 degree. It is assumed that the

pore pressure in the Slochteren Formation is only changing in the foot wall as a result of the operations.

The Norg subsurface parameters and in-situ stress have been assigned to different layers in the model as described section 5.2. Fault F2 is oriented perpendicular to the maximum horizontal stress (k_{0max} = 0.89), which is in contrast to Fault F1, which is oriented perpendicular to the minimum horizontal stress (k_{0min} = 0.85).

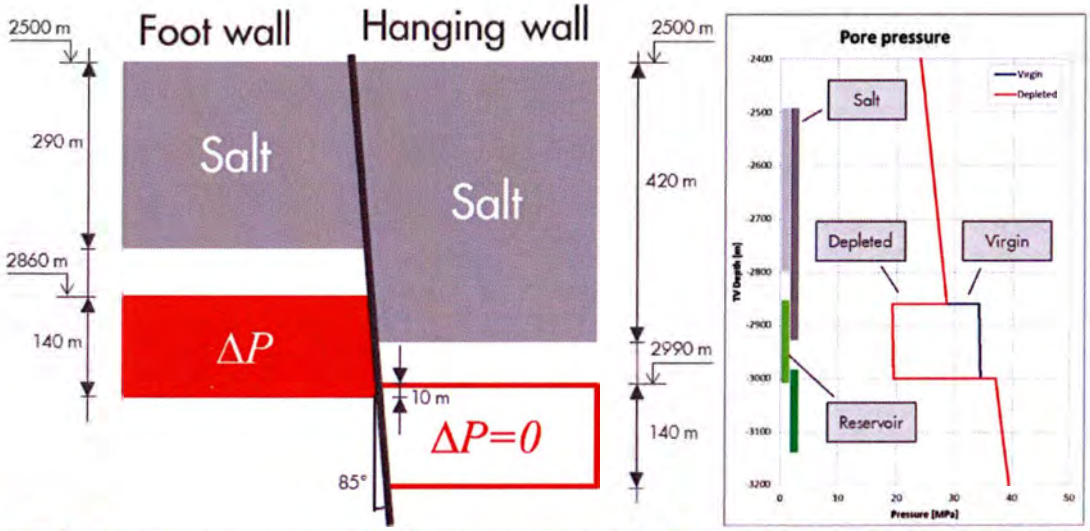

Figure 26 Simplified cross section used for the stability analysis of Fault F2. The Slochteren Formation is indicated in red, while the overlying non-depleting Ten Boer Member is white. Right the pore pressure distribution along the fault plane as a function of depth under virgin and depletion conditions.

The challenge is to select fault properties that simulate onset of seismic rupture only at the end of the re-pressurisation stage. Seismic rupture at the end of the initial depletion stage, as simulated for Fault F1, is to be prevented, because no seismic activity has been observed during depletion in the vicinity of this fault. This requires the fault to follow a different stress path under reservoir re-pressurisation compared to reservoir depletion. If not, the fault would return to the virgin reservoir conditions again, which is assumed to be stable.

In the current modelling approach, a different stress path along the fault plane can be enforced by assuming:

- a different set of elastic parameters during reservoir re-pressurisation compared to reservoir depletion, or by
- Developing a slip patch along the fault plane during depletion (without causing instability).

Different stress paths may also be caused by the evolvement of the pore pressure in the rock and faults during injection and depletion (see also section 4.3). This is considered to be a less likely scenario by the given high permeability of the reservoir rock. The first option is investigated in section 5.4.1, while the second option is addressed in sections 5.4.2 and 5.4.3.

5.4.1 Different elastic parameters during depletion and re-pressurisation

In this section, the impact on the stress path of different elastic parameters during the first depletion and re-pressurisation cycle is simulated for Fault F2 in the Norg UGS. That is, Young's modulus and

Poisson's ratio for the Slochteren Formation have been changed based on the experimental results obtained by de Kloe (2008), while elastic parameters of the other formations in the model were kept unchanged during re-pressurisation. Fault slip is suppressed by assuming a high value for the fault cohesion (10 MPa) and initial friction angle (0.6), so that the impact of the elastic parameters can be assessed in isolation.

In Case F2-1 (Table 9), Young's modulus and Poisson's ratio for all formations in the model are taken as summarised in Table 5 during the depletion *and* re-pressurisation stage of the field. In Case F2-2, the reservoir Young's modulus were increased by 15% and Poisson's ratio was increased by 4% during re-pressurisation in correspondence with the experimental results by de Kloe (section 3.2). In the third case, the elastic parameters were further increased to assess a more extreme hypothetical scenario. In case F2-3, Young's modulus is 36% larger and Poisson's ratio is 10% larger during re-pressurisation compared to depletion. It is highlighted that the elastic parameters are the same in all three cases during the depletion stage.

Table 9 Overview of model properties used.

	Young's modulus [GPa]		Poisson's ratio [-]	
Case	Depletion stage	Re-pressurisation Stage	Depletion stage	Re-pressurisation Stage
F2-1	14.7	14.7	0.227	0.227
F2-2	14.7	17.0	0.227	0.237
F2-3	14.7	20.0	0.227	0.250

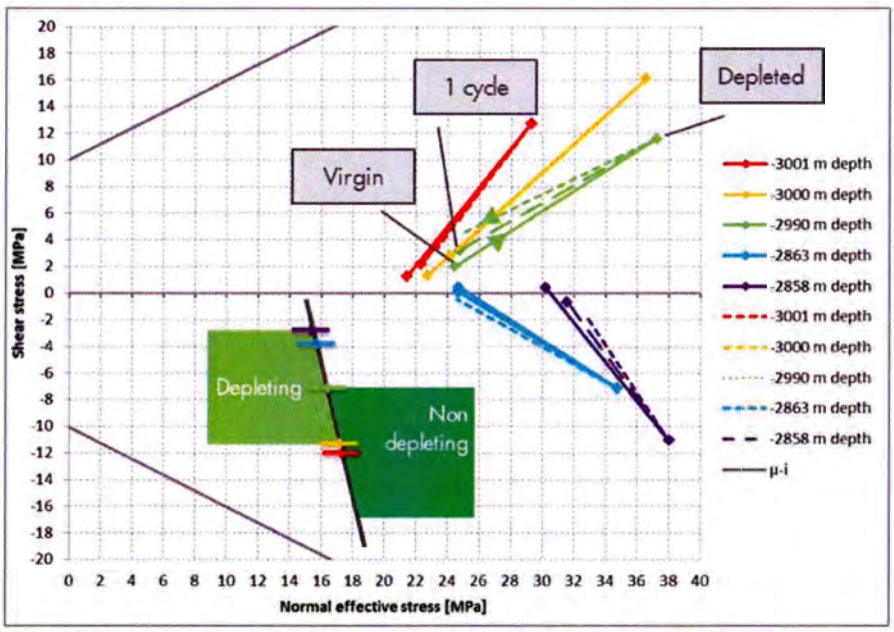

Figure 27 Stress paths for different points on the fault plane for Case F2-2 (solid lines) and case F2-3 (dashed). The insert shows the location of the stress paths. The start and end point of the stress path are indicated for the point at 2990 m depth. The grey lines indicate the onset of slip for a cohesion-less fault with initial friction coefficient of 0.6

The stress paths during re-pressurisation do not differ significantly from the stress paths during initial depletion when different elastic parameters are used. Figure 27 shows the stress paths of different points along the fault plane. The green line, which represents the stress path at the top of the depleting foot wall reservoir at 2990 m depth, shows most deviation between the depletion and

the re-pressurisation branch of the stress path. The arrow on the solid green line indicates the development of the normal and shear stress when the reservoir depletes with 15 MPa. Two dashed lines start in the depleted condition representing cases F2-2 and F2-3. Table 10 shows that this fault point returns to a shear stress of 3.3 MPa in case of F2-2 and 4.6 MPa in Case F2-3 after one depletion and re-pressurisation cycle, compared to a virgin shear stress 2.0 (Case F2-1). The difference in normal and shear stress condition before and after one cycle is smaller for the other points.

Table 10 Effective normal and shear stress calculated in three fault locations for different assumption of the elastic parameters during re-pressurisation.

	Normal stress [MPa]			Shear stress [MPa]		
Depth [m]	2858 m	2990 m	3000 m	2858 m	2990 m	3000 m
Virgin	30.2	24.4	22.7	0.4	2.0	1.4
15 MPa	38.0	37.2	36.5	-11.1	11.6	16.1
Re-pressurisation						
Case F1-1	30.2	24.4	22.7	0.4	2.0	1.4
Case F2-2	31.6	24.8	24.1	-0.7	3.3	2.8
Case F2-3	32.9	25.1	25.6	-1.9	4.6	4.4

From Figure 27 and Table 10 it is concluded that the calculated stress condition after depletion is significantly more critical than after a subsequent re-pressurisation cycle. The stress condition after depletion is closer to the Mohr-Coulomb shear failure line for any value of the initial friction coefficient. Therefore, it is concluded that using different elastic parameters for the Slochteren Formation does not contribute to the explanation of the seismic event that occurred after one depletion and re-pressurisation cycle on 7 June 1999.

5.4.2 Initial friction coefficient

In this section and the next, a different stress path is enforced by simulating stable, a-seismic slip during depletion that can lead to seismic rupture after re-pressurisation to the original reservoir pressure. This is done by adjusting the fault slip model outlined in section 5.2.

In the first series of analyses discussed in this section, the initial friction coefficient μ_i is adjusted to obtain onset of fault slip before 15MPa depletion (maximum depletion level in block 2) is reached. The residual friction coefficient μ_r is adjusted in the same fashion, so that the slope of the slip-weakening diagram remains unchanged (Figure 28). In next section, the critical slip displacement D_c is adjusted, while keeping the initial and residual friction coefficient the same. In this way, only the slope of the slip-weakening relationship is changed. The influence of the residual friction coefficient is discussed in the appendix. The fault cohesion of assumed to be zero in all analyses.

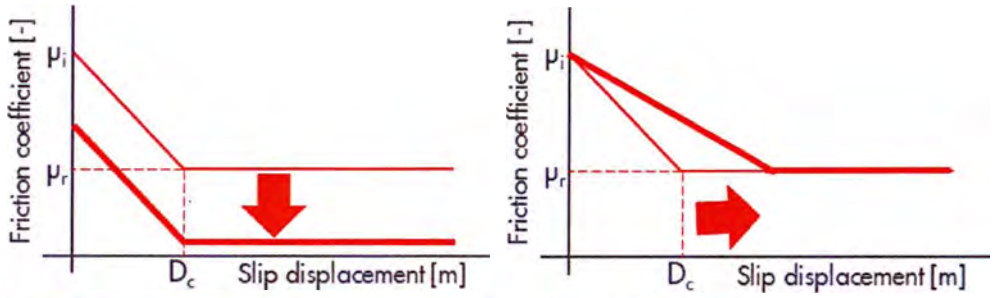

Figure 28 The linear fault slip-weakening relationship is changed by reducing
left: The initial and residual friction coefficient μ_i and μ_r respectively
right: The critical slip displacement D_c

First, the potential of a-seismic fault slip is explored for obtaining an alternative stress path under re-pressurisation compared to depletion. To this end, ten runs (F2-11 through F2-20) have been conducted with an initial friction coefficient in the range between 0.20 and 0.38. The slip weakening step has been assumed to have the same value in all analyses with a residual friction coefficient 0.15 lower than the initial friction coefficient. The critical slip displacement is D_c=0.01 m in all cases. This implies a reduction of friction coefficient per millimeter of fault slip of 0.015, i.e. a gradient of $\Delta\mu$ = -0.015 mm^{-1}.

Table 11 Onset of fault slip, onset of seismic rupture and fault properties in the first series of analyses.

Run	Initial friction coefficient μ_i [-]	Residual friction coefficient μ_r [-]	Critical slip displacement D_c [m]	Depletion at onset of fault slip [MPa]	Depletion at onset of seismic rupture [MPa]
F2-11	0.20	0.05	0.01	3.9	7.1
F2-12	0.22	0.07	0.01	4.6	8.3
F2-13	0.24	0.09	0.01	5.4	9.3
F2-14	0.26	0.11	0.01	6.1	10.7
F2-15	0.28	0.13	0.01	6.8	11.9
F2-16	0.30	0.15	0.01	7.7	13.1
F2-17	0.32	0.17	0.01	8.5	14.5
F2-18	0.34	0.19	0.01	9.3	> 15.0
F2-19	0.36	0.21	0.01	10.2	> 15.0
F2-20	0.38	0.23	0.01	11.1	> 15.0

The onset of fault slip starts at 3.9 MPa for an initial friction coefficient of 0.20 (Case F2-11) and at 11.1 MPa depletion for an initial friction coefficient of 0.38 (case F2-20, Table 11). The onset of fault slip is defined by the depletion level at which SCU=1 for at least one interface element, and marks the transition from an elastic, recoverable slip response to a plastic, irrecoverable fault slip response. The onset of fault slip and the length of the slip patch as a function of depletion are seen in right-hand side of Figure 29. The location and length of the slip patch at the end of the depletion stage, is shown in the left-hand graph. A reverse slip patch is nearly starting at the top of the depleting foot wall reservoir indicated by the SCU peak at a depth of 2860 m.

The onset of seismic rupture is reached at a depletion level smaller than 15 MPa for Cases F2-11 through F2-17 (Table 11). So, the objective to maintain a stable, a-seismic fault slip condition up to

15 MPa reservoir depletion is not met for an initial friction coefficient of 0.32 and smaller. Onset of seismic rupture is recognized by the vertical slope of the slip-depletion curve in the right-hand side of Figure 29, which implies that no incremental depletion is required to extend the size of the slip patch. For cases F2-18, through F2-20 (blue and purple curves in Figure 29) onset of seismic rupture has not been established, because reservoir depletion has been limited to 15 MPa (150 bar).

Irrecoverable fault slip is accumulated a-seismically after the onset of fault slip in all cases. The slip patch develops at the bottom of the foot wall in all cases (red circle in the left-hand graph) and develops upward and downwards along the fault plane. The graph shows the fault slip condition at the onset of seismic rupture. It is seen that the length of the slip patch is largest for case F2-11 with the smallest initial friction coefficient. A second peak in the SCU value is seen at the top of the hanging wall in all cases, but does not reach slip conditions (SCU=1).

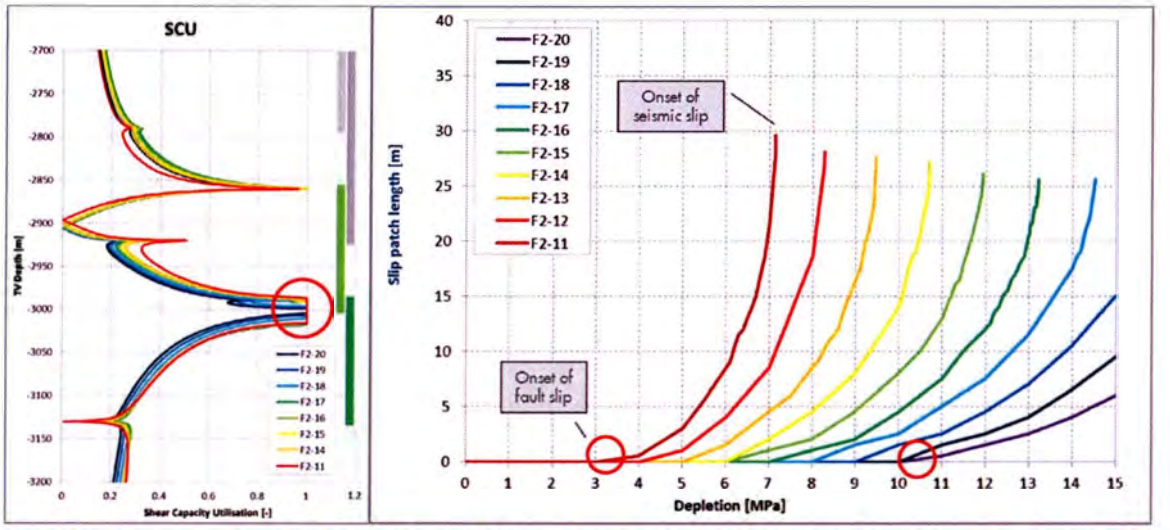

Figure 29 Left: the Shear Capacity Utilisation (SCU) as a function depth at the onset of seismic rupture. The red circle highlights the interval where fault slip occurs (SCU=1).
Right: the length of the slip patch as a function of depletion for all the analyses listed in Table 11. The analysis are terminated at the onset of seismic rupture for an initial friction coefficient of 0.32 or smaller, and at 15 MPa depletion for a friction coefficient larger than 0.32. Red circles indicate onset of a-seismic fault slip for case F2-11 and F2-20.

This series of analyses shows that

- Onset of (a-seismic) fault slip is calculated at a lower depletion level for a smaller value of the initial friction coefficient
- Onset of seismic rupture also starts at a lower depletion level for a smaller value of the initial friction coefficient
- The initial friction coefficient should be at least 0.34 to prevent onset of seismic rupture to occur at a depletion level smaller than 15 MPa with a drop in friction coefficient of 0.15 with a gradient of $\Delta\mu = -0.015\ mm^{-1}$.

More ductile fault slip behaviour is required to prevent seismic rupture to occur at a depletion level below 15 MPa for cases F2-11 through F2-17. This can be achieved by increasing the critical slip displacement D_c, which causes the descending branch in the slip-weakening diagram to become less steep (Figure 28). This response can be explained by considering the extreme case if $D_c = 0$ and a sufficiently small the residual friction coefficient. In that case seismic rupture occurs at the same

depletion as the onset of fault slip, because the fault strength suddenly becomes too low to carry the shear stress on the fault plane. No seismic rupture occurs in the other extreme case if D_c is infinite. This case implies that no slip-weakening materialises, which prevents the fault becoming unstable (van den Bogert, 2015). Buijze (2015) also showed that a larger value for D_c requires a larger slip patch to reach instable equilibrium. In the next section, the critical slip displacement D_c is increased in order to maintain stable fault slip during depletion the depletion stage of the Norg UGS.

5.4.3 Slope of the fault slip-weakening diagram

The cases in the previous section are repeated for a critical slip displacement D_c of 0.02 m instead of 0.01 m. This implies a reduced slope in the slip-weakening diagram from $\Delta\mu$ = -0.015 mm^{-1} to $\Delta\mu$ = -0.0075 mm^{-1}, were $\Delta\mu$ expresses the reduction of friction coefficient per millimetre of fault slip displacement. The objective is to maintain an a-seismic slip condition up to a reservoir depletion of 15 MPa (Table 12).

Table 12 Onset of fault slip, onset of seismic rupture and fault properties in the second series of analyses.

Run	Initial friction coefficient μ_i [-]	Residual friction coefficient μ_r [-]	Critical slip displacement D_c [m]	Depletion at onset of fault slip [MPa]	Depletion at onset of seismic rupture [MPa]
F2-21	0.20	0.05	0.02	3.9	> 15.0
F2-22	0.22	0.07	0.02	4.6	> 15.0
F2-23	0.24	0.09	0.02	5.4	> 15.0
F2-24	0.26	0.11	0.02	6.1	> 15.0
F2-25	0.28	0.13	0.02	6.8	> 15.0
F2-26	0.30	0.15	0.02	7.7	> 15.0
F2-27	0.32	0.17	0.02	8.5	> 15.0

The results in the last column of Table 12 show for all cases that the fault remains stable beyond a reservoir depletion of 15 MPa if the critical slip displacement is 0.02 m. Onset of fault slip starts at the same depletion level as in the first series of analyses. This is expected, because the critical slip displacement D_c affects only the post-failure behaviour of the fault. Comparison between Figure 30 and Figure 29 shows that the slip patch develops slower after the onset of fault slip for D_c=0.02 m than for D_c=0.01 m, and that the slip patch size can increase significantly without the fault becoming unstable.

The right-hand side of Figure 30 shows that the slip patch extends much further in the upward and downward directions, starting at the bottom of the depleting foot wall reservoir. In this series of analyses, also a slip patch is formed at the top of the foot wall reservoir. This is a reverse slip motion that prevents the main slip patch from propagating upwards, and is also the reason why the main slip path extends further downwards than upwards.

The parameters in Table 12 allow Fault F2 to slip and to develop irrecoverable deformation, while preventing it from becoming unstable. This corresponds with the observation that no seismic event has occurred until the reservoir is fully re-pressurised at this location. Analyses are continued by increasing the reservoir pressure again to virgin reservoir conditions, simulating re-pressurisation during the storage cycle.

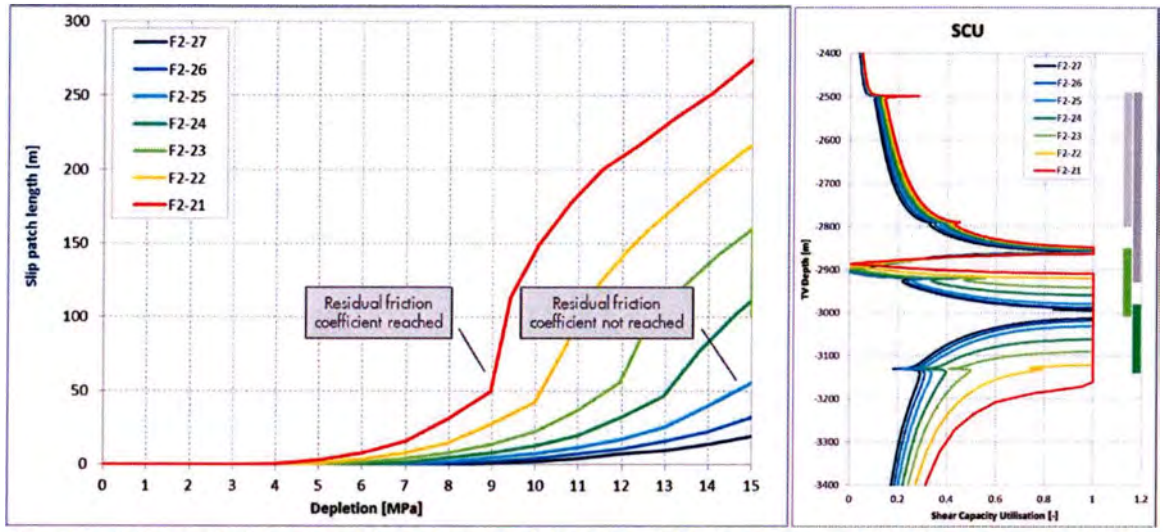

Figure 30 Left: Length of the slip patch as a function of depletion. Right: Shear Capacity Utilisation as a function depth for the all analyses listed in Table 12.

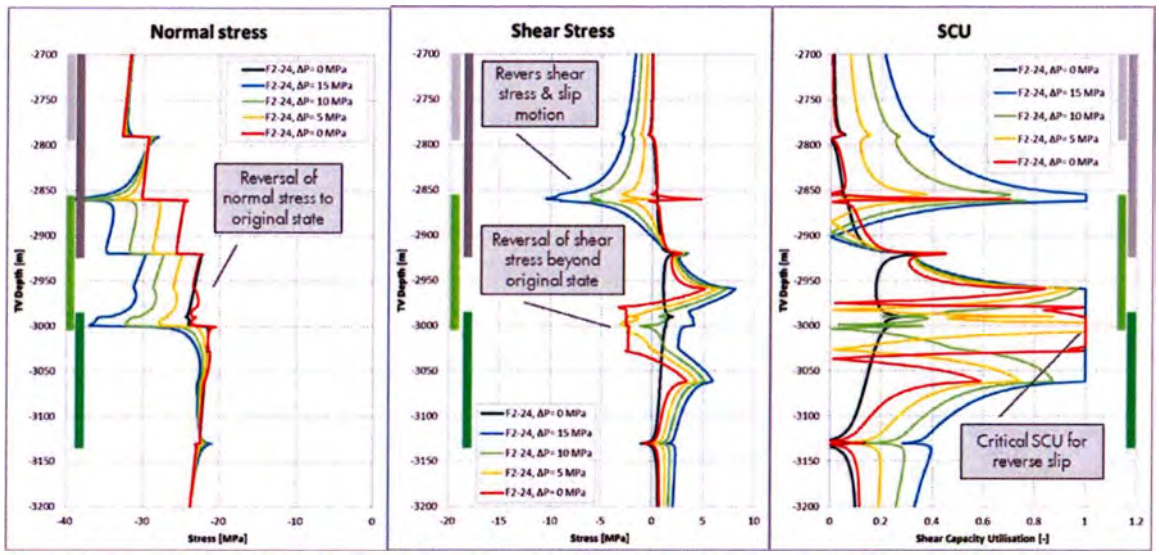

Figure 31 Normal stress, shear stress and Shear Capacity Utilisation as a function depth for case F2-24 for a re-pressurisation of 0 MPa (15 MPa depletion), 5 MPa (10 MPa depletion), 10 MPa (5 MPa depletion) and 15 MPa (0 MPa depletion). The dark blue line represents the virgin reservoir condition before initial depletion. Negative normal stress indicate compression, negative shear stress is directed upward.

Figure 31 shows the (effective) normal and shear stress distribution and Shear Capacity Utilisation (SCU) along the fault plane during the re-pressurisation of the foot wall reservoir (case F2-24). The light blue lines represent the condition at the beginning of the storage stage of the Norg UGS, when the reservoir pressure is depleted by 15 MPa (150 bar). The dark blue line represents the virgin reservoir condition before any depletion has taken place, while the red line represents the condition at the end of a complete depletion & re-pressurisation cycle when reservoir is back at the original pressure again. The differences between the red and dark blue lines are hence caused by the irrecoverable deformation of the fault. It is seen that the effective normal stress (left-hand graph) is virtually returning to virgin reservoir conditions, while shear stress and SCU are distinctly different from virgin due to fault slip accumulated during the initial depletion stage.

Two slip patches are recognised in the right-hand graph at the beginning of the re-pressurisation stage (SCU=1, light blue line at 15 MPa depletion). The negative shear stress at the top of the depleting foot wall reservoir at the beginning of the re-pressurisation stage (middle graph) confirms the reverse slip movement. The main slip patch at the bottom of the foot wall reservoir slips in normal direction (positive/downward shear stress). Re-pressurisation of the foot wall reservoir to original reservoir pressure causes the shear stress to change direction over the slip patch created during the depletion stage (red line in middle graph). Fault slip is simulated is reverse direction (SCU=1) before pressure is back at 0 MPa depletion (yellow and red lines in right-hand graph).

The following is found by comparing the simulated fault condition after one depletion and re-pressurisation cycle with the condition in the virgin state:

- the normal (effective) stress virtually returns to the virgin stress state
- reverse shear stress is observed after one depletion & re-pressurisation cycle
- reverse shear stress can lead to reverse fault slip over a part of the fault

Figure 32 shows the significant impact of fault slip on the stress path of various points on the main slip patch. In this p-q plot, the fault normal stress is plotted on the horizontal axis and the resultant shear stress on the vertical axis for several stages in the depletion and re-pressurisation cycle. The initial and residual friction coefficient are plotted as solid resp. dashed grey lines. The virgin shear stress condition is positive (downward) and lies well below the initial and also the residual fault strength. The stress path of the points in the Rotliegend juxtaposition interval (insert in Figure 32) hit the initial failure line during depletion and cause onset of fault slip. Ongoing depletion and fault slip causes the stress path to continue towards the line of residual fault strength due to the prescribed slip-weakening model. Subsequent re-pressurisation of the reservoir to the original reservoir pressure causes the shear stress to change direction, become negative and hit the residual shear failure line causing reverse fault slip. Note that the points at the top of the foot wall reservoir (blue and purple lines) do not show substantial slip and slip-weakening during depletion. The stress paths of these points are more or less the same under depletion and re-pressurisation.

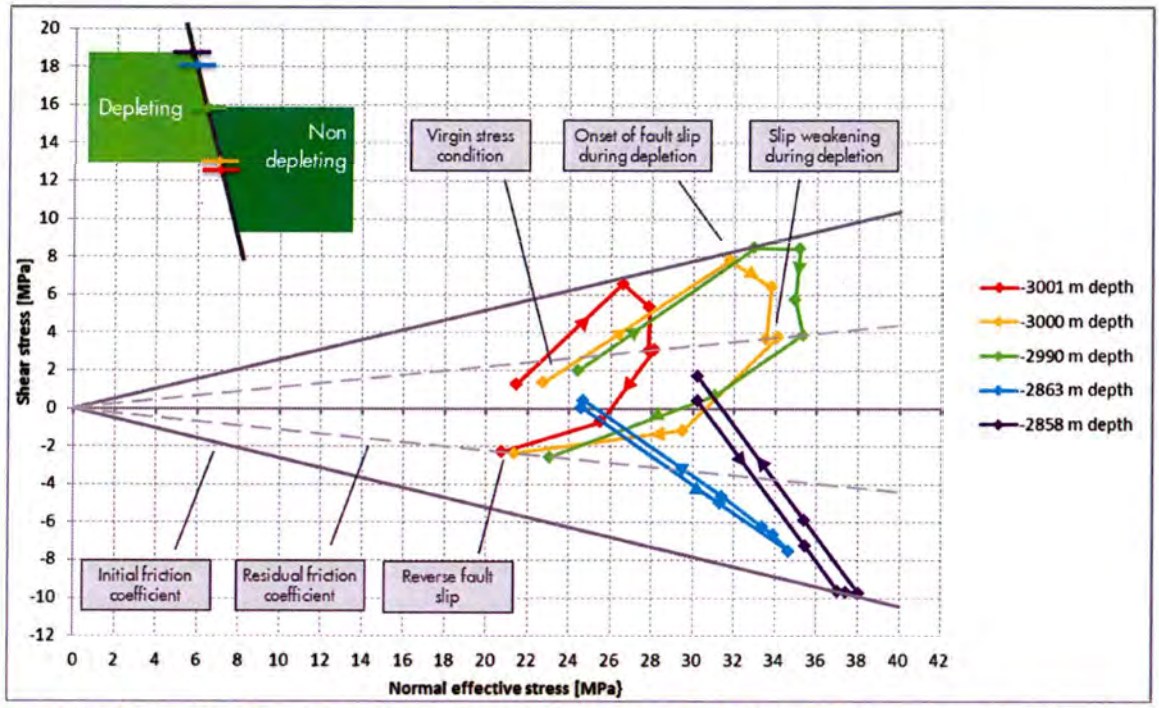

Figure 32 Stress paths of several points along the fault plane for case F2-24. Upper left picture gives an indication of the positions of the points that were selected for the graphs. Arrows indicate the stress path followed during depletion and re-pressurisation.

The fact that reverse fault slip is simulated after completion of one depletion and re-pressurisation cycle implies that fault slip can also occur seismically. The employed fault slip relationship (Figure 19 in section 5.2) allows for weakening during the first loading cycle, which occurs in downward direction during the depletion stage of the field. The fault slip relationship assumes the same friction coefficient if the shear direction is reversed. However, it is reasonable to assume that granular material like the Slochteren Formation demonstrates different frictional slip behaviour under reversal of the shear direction. Also, it not unrealistic to assume that stick-slip behaviour can occur again under reversed slip. In other words: a different slip relationship could be considered for reverse fault slip that includes further slip weakening and associated instable (seismic rupture).

It is concluded that accumulation of a-seismic slip during the depletion stage of the Norg UGS might explain the occurrence of the seismic event on Fault F2 in June 1999 after completion of the full re-pressurisation cycle. The hypothesis of different elastic parameters during re-pressurisation compared to depletion cannot explain the seismic event, because the stress paths during both stages are virtually the same.

5.5 Summary and discussion of the results

In section 5.3, a model hypothesis has been developed that simulates the first seismic event on Fault F1 in March 1993 during the initial depletion stage of the Norg USG. This hypothesis assumes:

- A juxtaposition of the depleting block 2 reservoir against Zechstein rock salt across Fault F1
- A minimum horizontal stress ratio k_{0min} of 1 in the Zechstein salt and 0.85 for all other formations
- An initial fault friction coefficient between 0.25 and 0.29
- A slip-weakening relationship with critical slip displacement between 1 and 5 mm.

It is found that a rather weak and brittle fault slip response is required to reproduce the seismic event on the boundary fault of the Norg UGS. An initial friction coefficient smaller than 0.30 is considered weak, considering the fact that many fault reactivation studies (Byerlee 1978, Di Torro 2011) assume a default value of 0.60. A critical slip displacement of a few millimetres is rather brittle considering the fact that slip displacement can reach several centimetres of even decimetres depending on the size of the slip patch. Nevertheless, this fault response could be feasible by the potential presence of salt that could explain the rather low strength of the fault zone and the presence of the Slochteren sandstone that could form brittle asperities that could fail under small deformations (Urai et al., 2016). The combination of small slip patches and low values for the initial friction coefficient could indicate a larger likelihood for small earthquakes as observed in the Norg UGS in the past. This observation largely depends on the assumption of a relative small ambient shear stress.

The model hypothesis allows for multiple locations on the fault plane that could be the source of the 1993 seismic event. In section 5.3 it is shown that the high horizontal stress assumption associated with salt suppresses potential slip location locations at the top and bottom of the reservoir in block 2. However, uncertainty and variability of fault and formation properties could still explain occurrence of the event on these locations. This part of the hypothesis cannot be verified in the absence of more accurate source location data.

In section 5.4, a model hypothesis has been developed that simulates the second seismic event in the Norg USG in June 1999. The challenge in this scenario is to formulate a stress path that brings Fault F2 to criticality under near-virgin reservoir conditions after a depletion and re-pressurisation cycle without seismic rupture, while the virgin fault is considered stable. The following model hypothesis does satisfy these requirements

- A partial juxtaposition of the depleting block 2 reservoir against Zechstein rock salt across Fault 2
- A minimum horizontal stress ratio k_{0min} of 1 in the Zechstein salt and 0.89 for all other formations
- An initial fault friction coefficient between 0.20 and 0.32
- A slip-weakening relationship with critical slip displacement of about 20 mm or more

The hypothesis is based on the development of a different stress path under re-pressurisation compared to reservoir depletion conditions. It is found that a-seismic fault slip during depletion can enforce a significantly different stress path under re-pressurisation. Reverse fault slip with the potential of becoming seismic is simulated under near-virgin reservoir pressure as a consequence of the alternative stress path. A relatively low initial friction angle and relatively large critical slip displacement are required in order to simulate fault slip under depletion that does not become seismogenic. Furthermore, it is found that different elastic parameters (Young's modulus and Poisson's ratio) for depletion and re-pressurisation do not lead to a different stress path that could explain seismic rupture after one depletion and re-pressurisation cycle.

6 Conclusions and Recommendations

This report addresses the potential seismic threat for the Norg UGS. Both qualitative and quantitative considerations that are described in this report conclude that the seismic threat and therefore also the seismic risk are low. This is supported by the following statements:

- Only two small events on boundary faults have been observed over the whole operational period of the Norg UGS
- No seismicity was observed over the last 17 years with high variation of production- and injection (rates)
- The main physical explanations that support this observation are;
    - High permeability of the reservoir rock and therefore no relative pressure build-up in the fault plane
    - Small temperature differences between the injected gas and reservoir rock
    - Production and injection rates do not show an obvious correlation with seismicity
    - Low ambient shear stress level observed from the in-situ Norg leak-off test
- The findings from the numerical studies that support the main conclusion are:
    - The observed seismic events can be explained by low fault strength (initial friction coefficient), which is considered at the tail end of the probability distribution.
    - If any, slip could have occurred a-seismically on various faults in the Norg UGS. However, rather ductile fault behaviour is to be expected to explain the absence of seismic events.
    - Any difference in stress paths induced by fault slip or induced by other mechanisms under depletion and re-pressurisation, did not cause seismic events in the last 17 years
    - Difference in elastic parameters of the Slochteren Formation does not cause a significant difference in stress paths under depletion and re-pressurisation.

A-seismic fault slip is considered to be the main source for the development of a different stress path under depletion and re-pressurisation. If any, fault slip must have occurred a-seismically in view of the absence of seismic events over the last 17 years. Different elastic response can be excluded as a source for a significantly different stress path.

Therefore, based on field observations, laboratory measurements and model hypothesis, current expectation is that stress paths will remain (virtually) the same under depletion and re-pressurisation and that the likelihood of seismic events is small within the entire historical reservoir pressure range.

7 References

Buijze, L., Orlic, B., Wassing, B.B.T. (2015), *Modelling fault rupture in a depleting gas field*. Report TNO project report 2015 R10844, November 2015.

Byerlee, J.D. (1978), Friction of Rocks, Pure Appl. Geophys., Vol. 116, pp. 615-626.

de Kloe K.P., van der Linden A.J., Dudley J.W. (2008) Cyclic Compaction Experiments on Samples from Norg-5. Shell report, EP 2008-5189.

Di Torro, G., Han, R., Hirose, T. De Paola, N., Nielsen, S., Mizoguchi, K., Ferri, F., Cocco, M., and Shimamoto, T. (2011), Fault Lubrication during earthquakes, Nature, Vol. 471, March 2011.

Nagelhout, A.C.G.& Roest, J.P.A., Geomechanical modelling of the Norg gas field, 1997; TU-Delft. TA/IG/97.51 Centre of Technical Geoscience.

NRD-01 (1995) FST test https://eu001-sp.shell.com/sites/AAAAB0326/_layouts/15/WopiFrame.aspx?sourcedoc=/sites/AAAAB0326/Lib01/00000037%20(NAM200408169488).pdf&action=default&DefaultItemOpen=1

TNO (2016 a) Literature review on Injection-Related Induced Seismicity and its relevance to Nitrogen Injection,TNO-rapport 2014 R11761, 18 december 2014.

TNO (2016 b) Description and analysis of field cases of injection in The Netherlands. TNO-rapport 2015 R10906, 5 november 2015.

TNO (2016 c) Geomechanical modelling of the effects of (nitrogen) injection on fault stability in a reservoir, representative for a typical Rotliegend reservoir in the northern part of The Netherlands TNO-rapport 2015 R11259, 11 november 2015.

Urai, J. L. Kettermann M., Abe S., Virgo S. (2016) Aspects of fault zones around the Rotliegend reservoirs and the possible effects of salt in the fault zones on rates of seismicity in these zones. Report of a short project in April - May 2016.

Van Eijs (2015) Neotectonic Stresses in the Permian Slochteren Formation of the Groningen Field. NAM report EP201510210531.

Van den Bogert, P.A.J. (2015), Impact of various modelling options on the onset of fault slip and fault slip response using 2-dimensional Finite-Element Modelling. Report SR.15.11455, Shell Global Solutions International B.V.

Zheng, Y. and Guises, R. (2013) Dynamic geomechanical modelling to assess and minimize risk for fault slip during reservoir depletion of the Groningen field; 1D Geomechanical study. Baker Hughes report NAM0001.

Enclosure-1 Cross sections

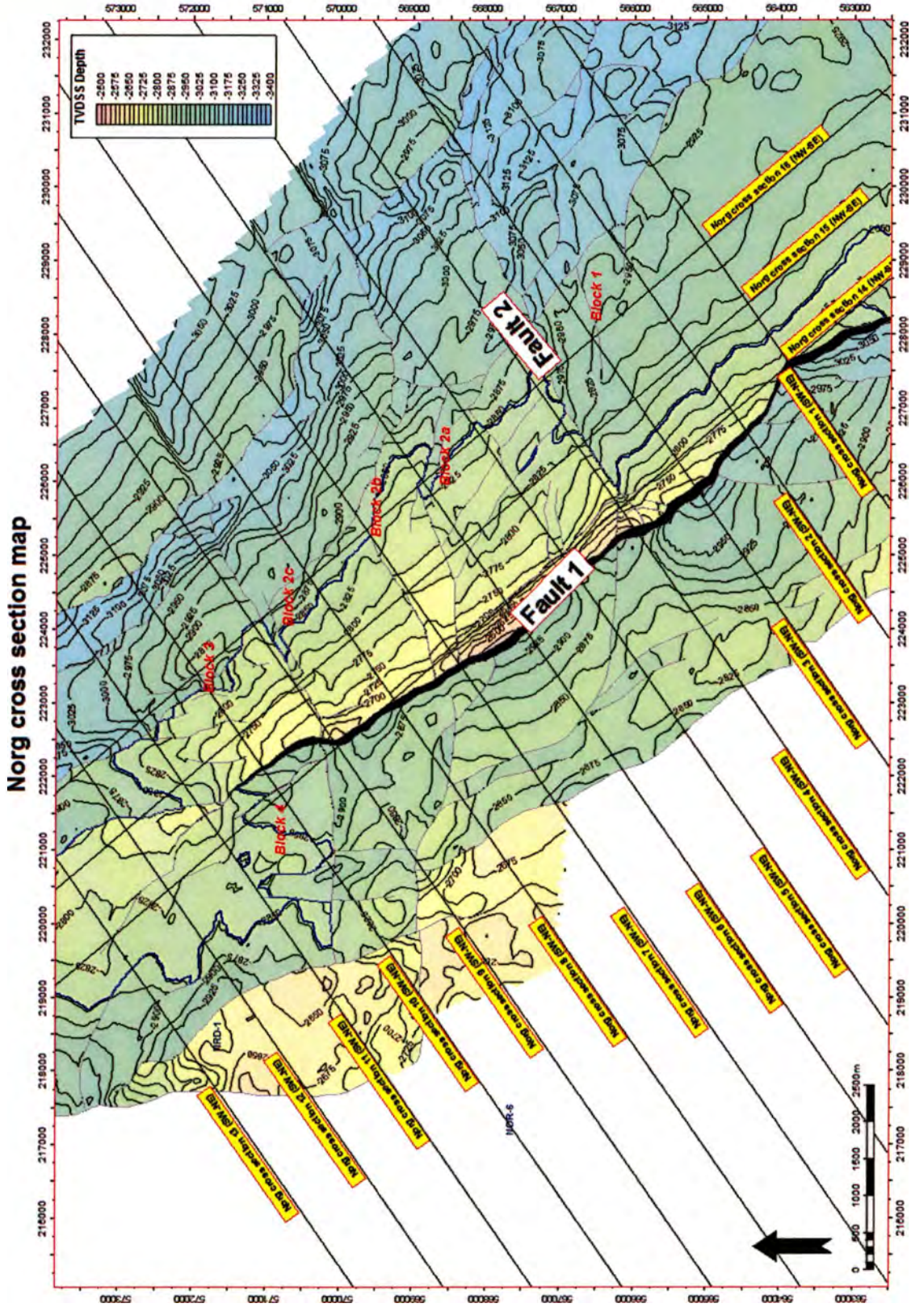

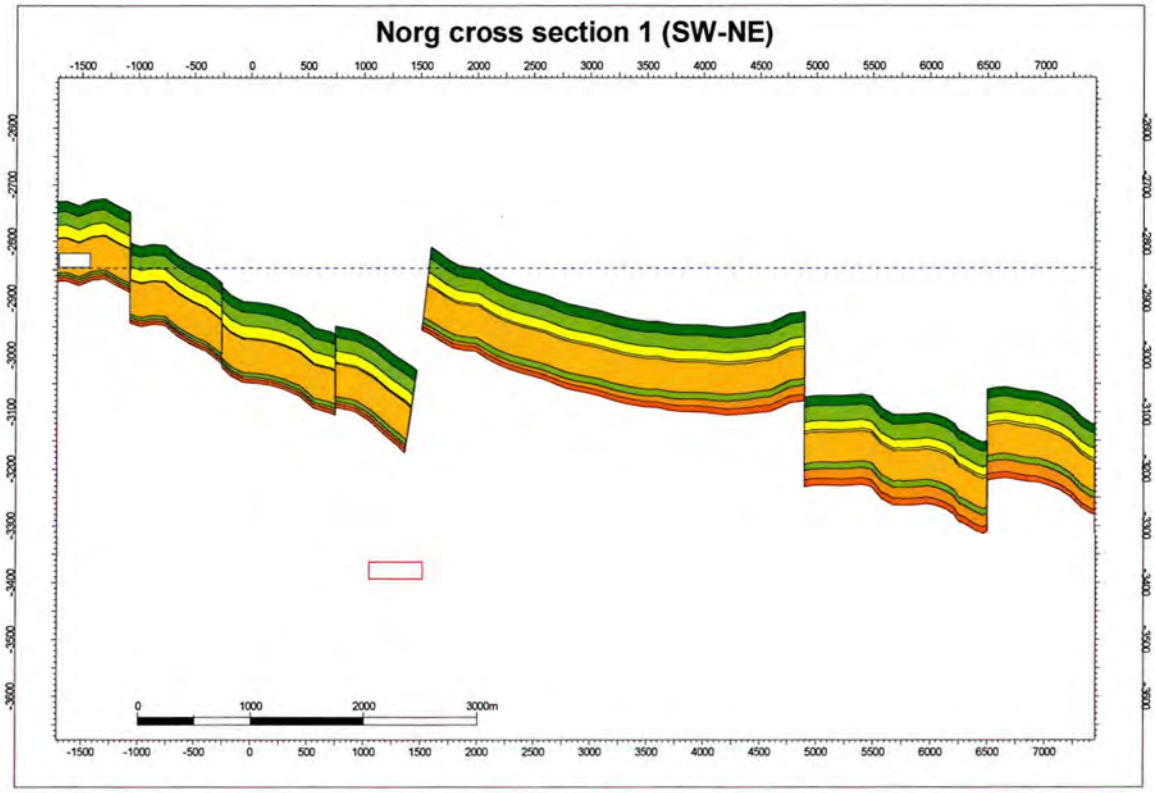
Norg cross section 1 (SW-NE)
-1500 -1000 -500 0 500 1000 1500 2000 2500 3000 3500 4000 4500 5000 5500 6000 6500 7000
-2600 -2700 -2800 -2900 -3000 -3100 -3200 -3300 -3400 -3500 -3600
0 1000 2000 3000m

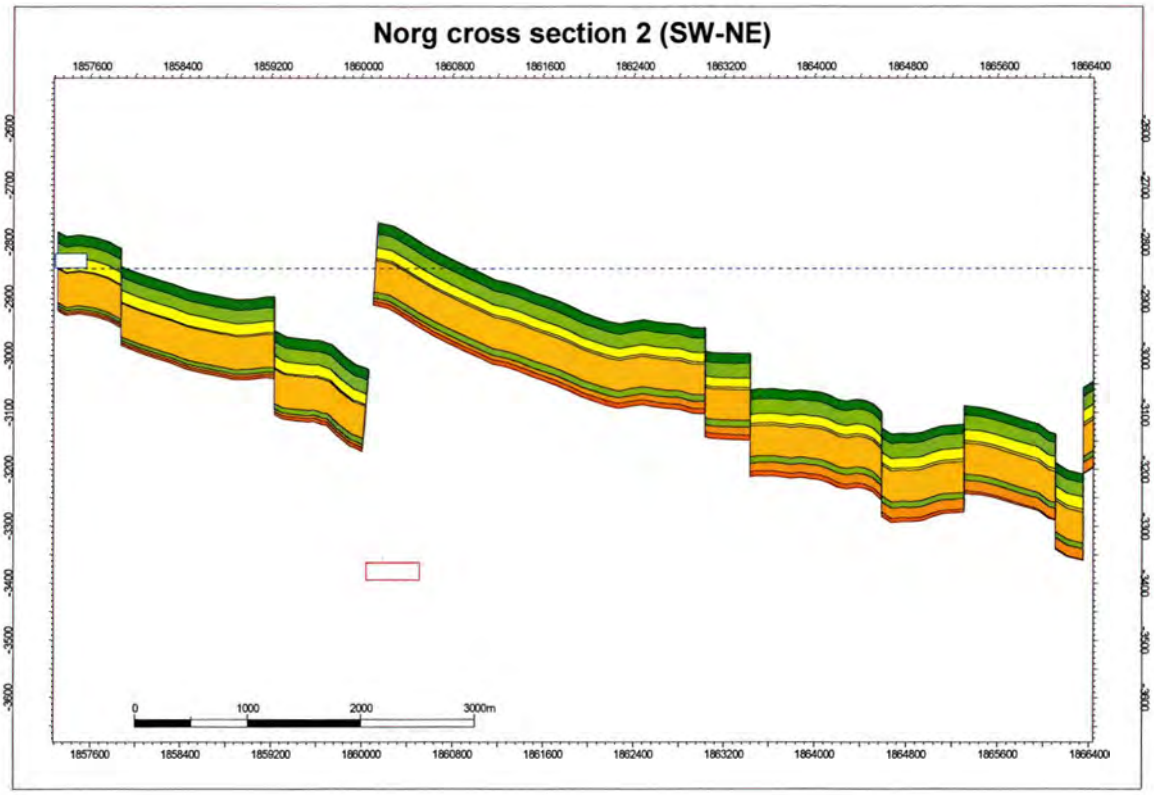
Norg cross section 2 (SW-NE)
1857600 1858400 1859200 1860000 1860800 1861600 1862400 1863200 1864000 1864800 1865600 1866400
-2600 -2700 -2800 -2900 -3000 -3100 -3200 -3300 -3400 -3500 -3600
0 1000 2000 3000m

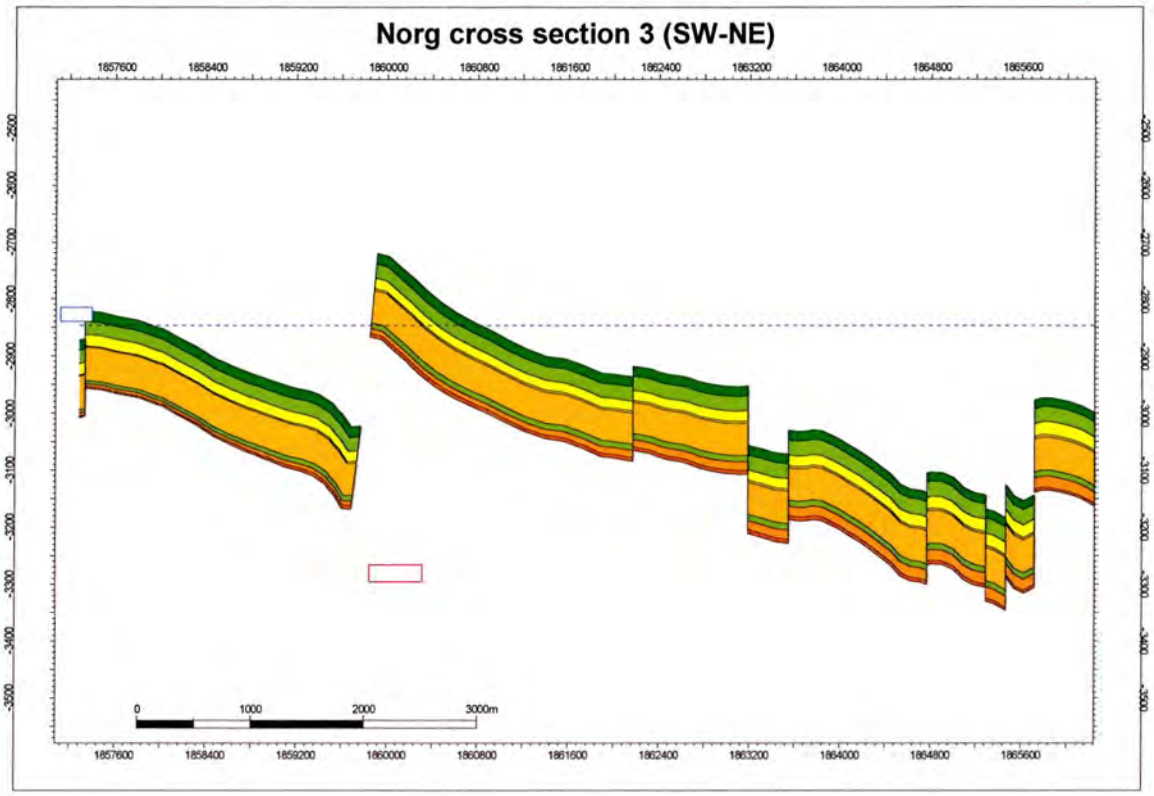
Norg cross section 3 (SW-NE)
1857600
1858400
1859200
1860000
1860800
1861600
1862400
1863200
1864000
1864800
1865600
2500
2600
2700
2800
2900
3000
3100
3200
3300
3400
3500
0
1000
2000
3000m

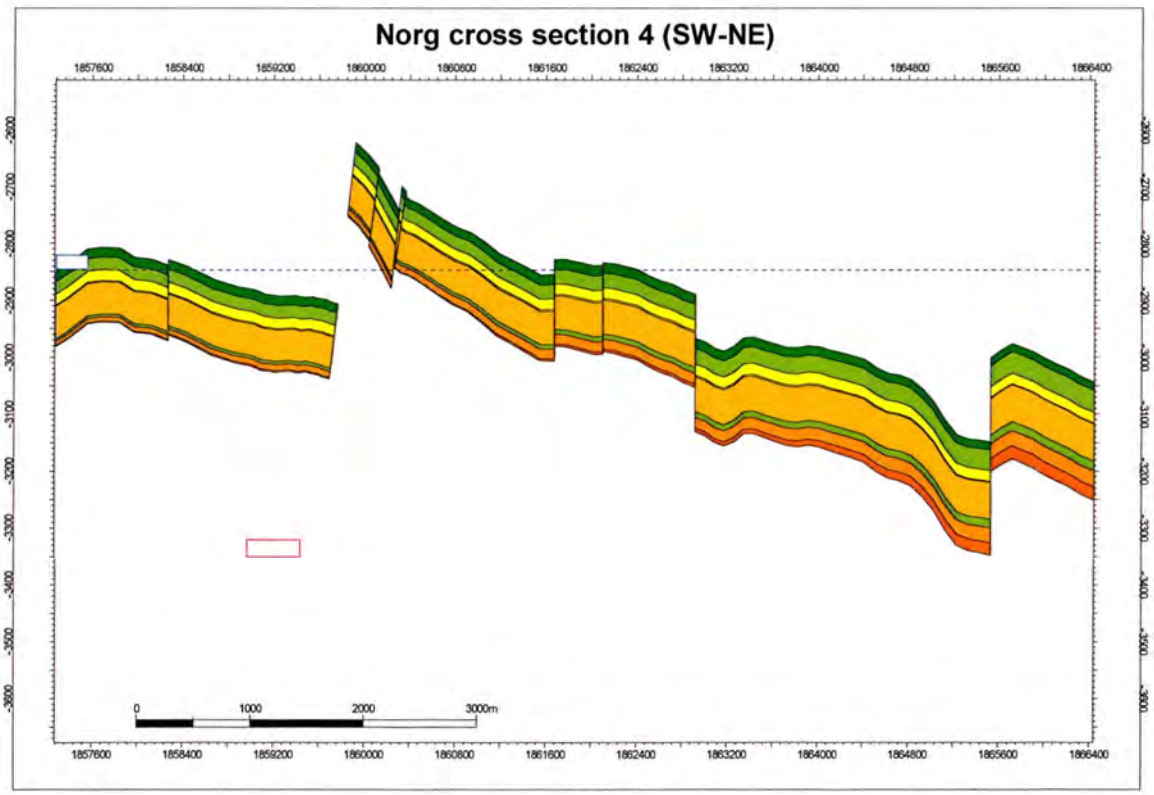
Norg cross section 4 (SW-NE)
1857600
1858400
1859200
1860000
1860800
1861600
1862400
1863200
1864000
1864800
1865600
1866400
2600
2700
2800
2900
3000
3100
3200
3300
3400
3500
3600
0
1000
2000
3000m

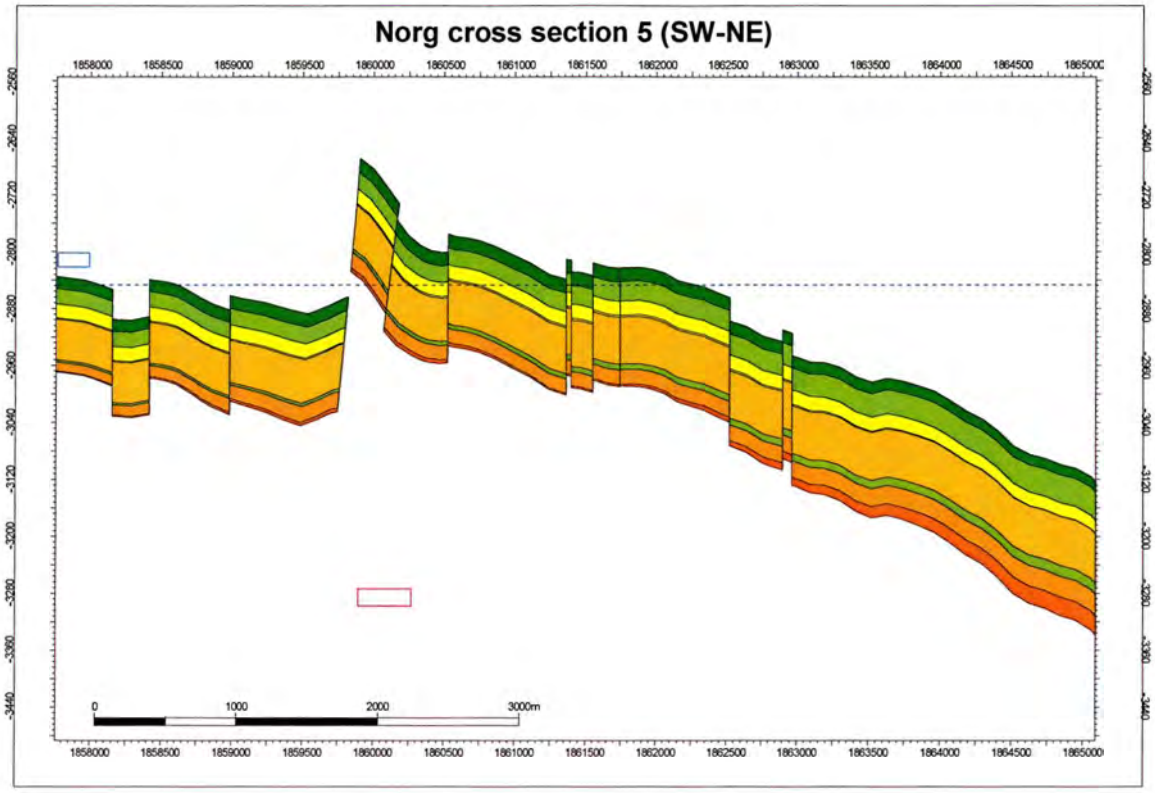
Norg cross section 5 (SW-NE)
1858000
1858500
1859000
1859500
1860000
1860500
1861000
1861500
1862000
1862500
1863000
1863500
1864000
1864500
1865000
0
1000
2000
3000m

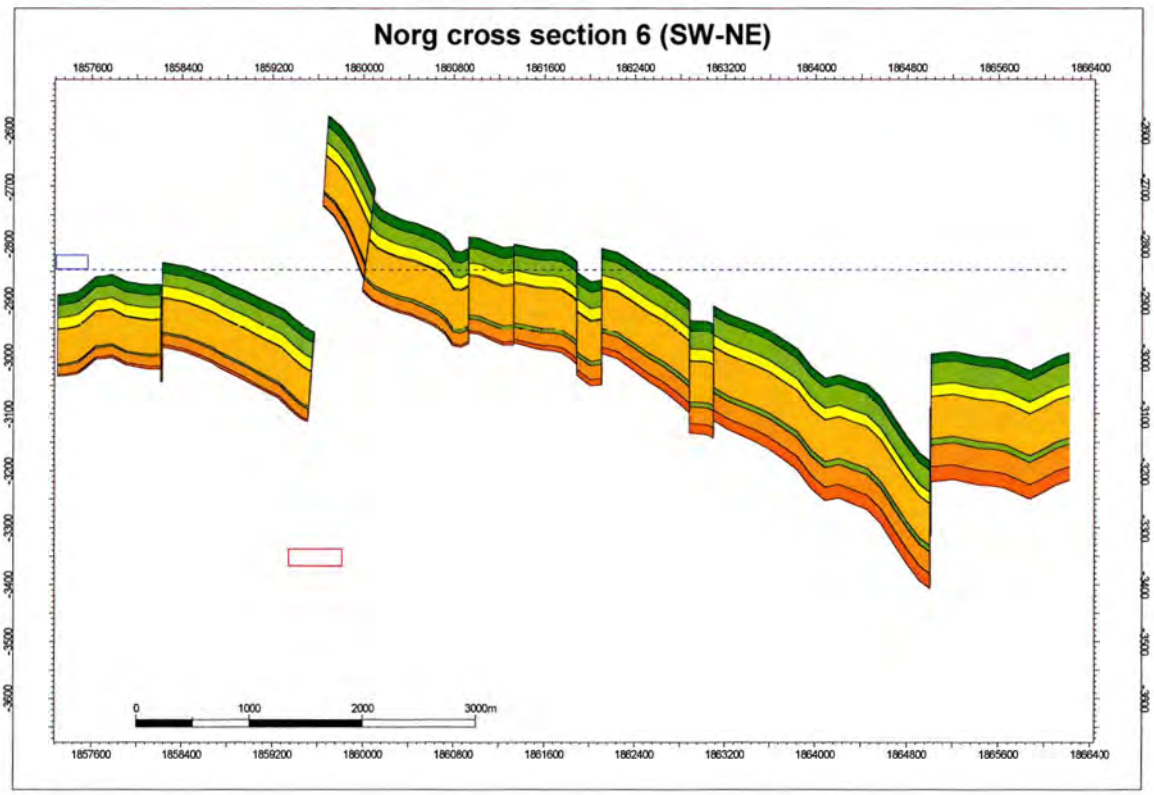
Norg cross section 6 (SW-NE)
1857600
1858400
1859200
1860000
1860800
1861600
1862400
1863200
1864000
1864800
1865600
1866400
0
1000
2000
3000m

Norg cross section 6 (SW-NE)

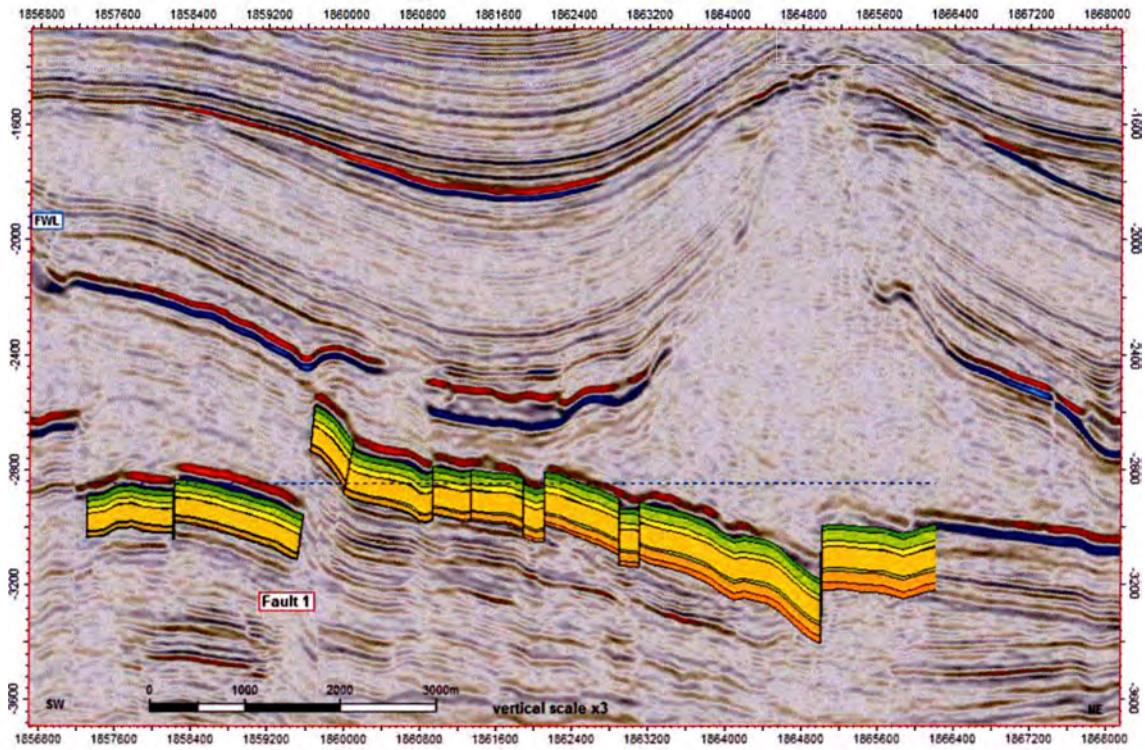

Norg cross section 7 (SW-NE)

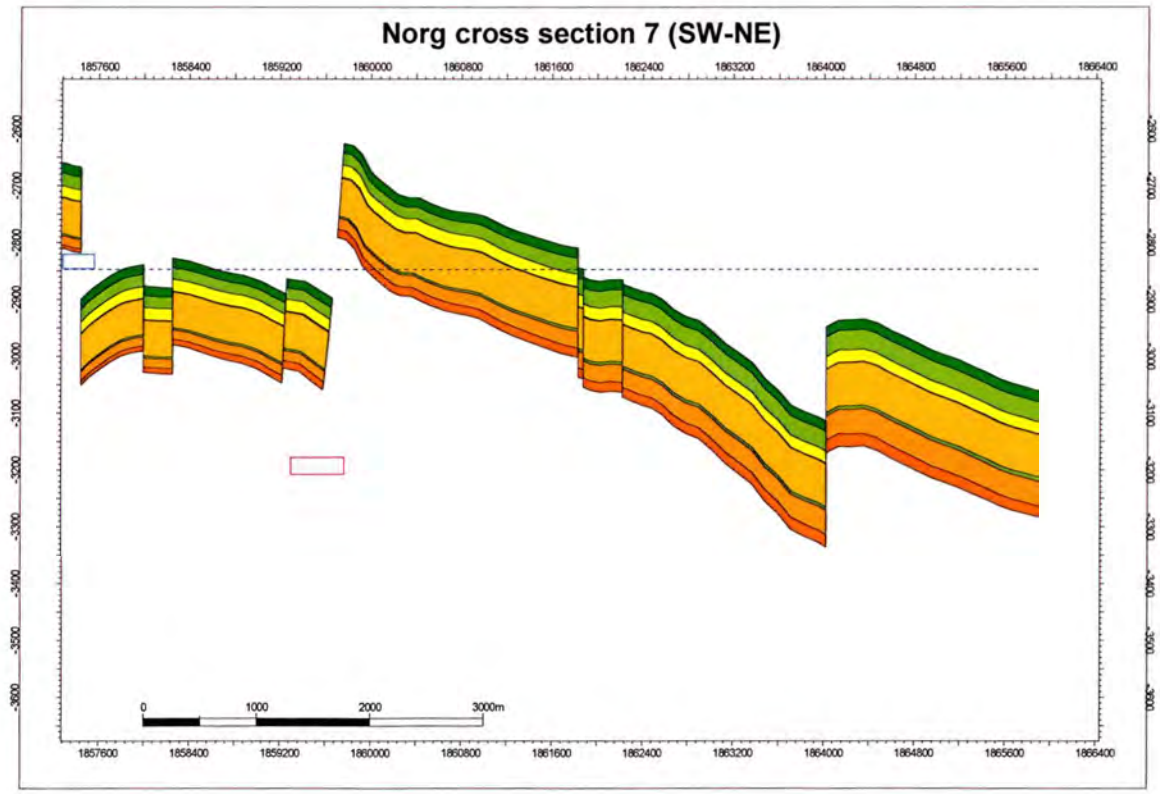

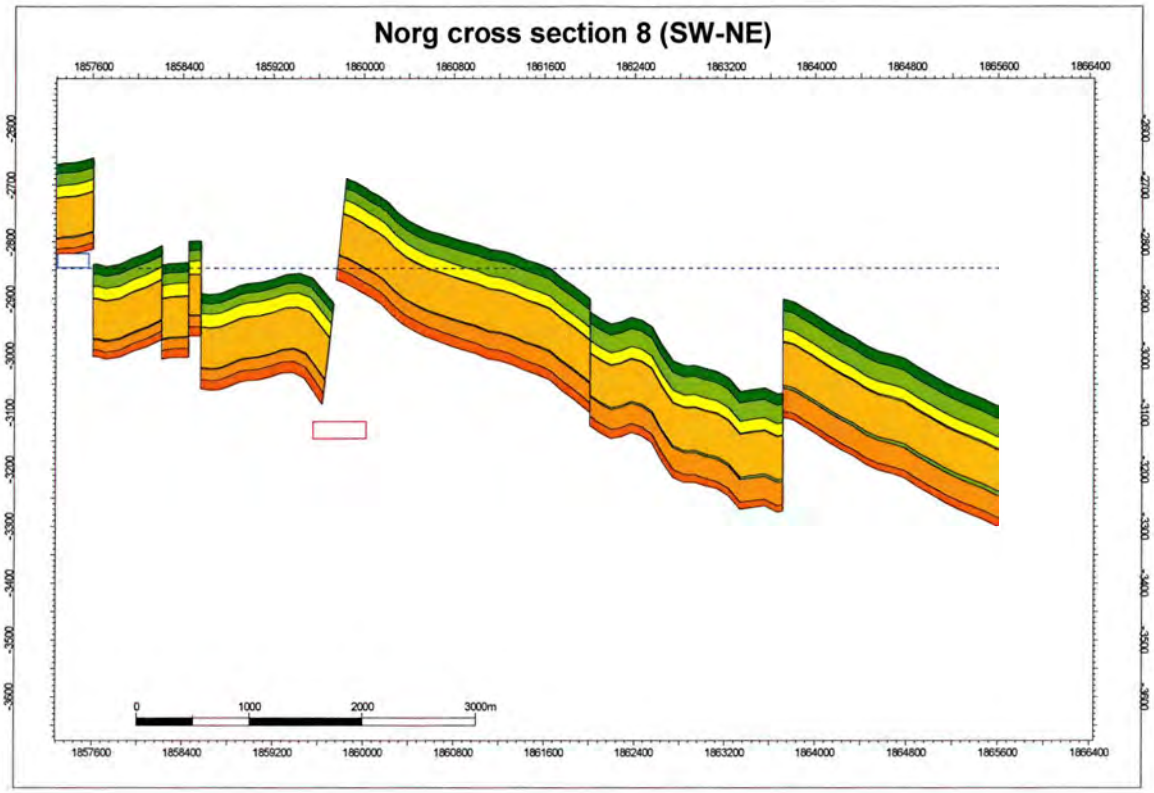
Norg cross section 8 (SW-NE)
1857600
1858400
1859200
1860000
1860800
1861600
1862400
1863200
1864000
1864800
1865600
1866400
0
1000
2000
3000m

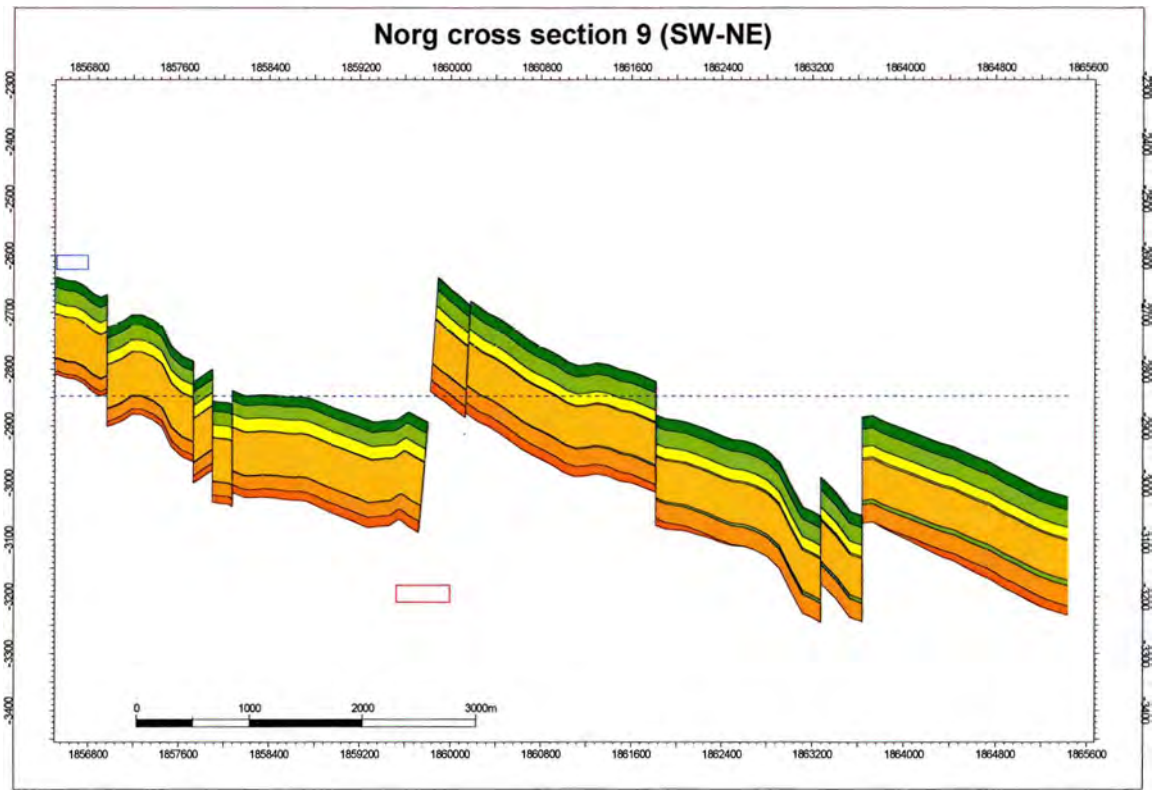
Norg cross section 9 (SW-NE)
1856800
1857600
1858400
1859200
1860000
1860800
1861600
1862400
1863200
1864000
1864800
1865600
0
1000
2000
3000m

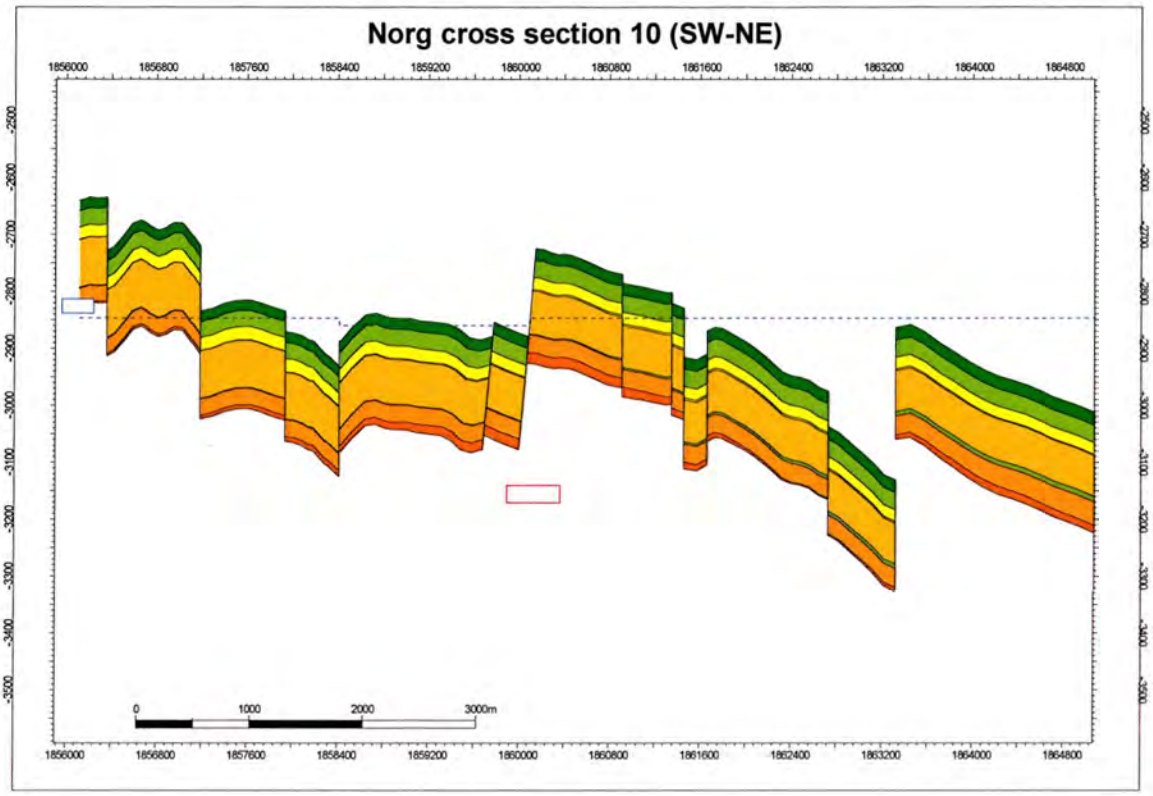
Norg cross section 10 (SW-NE)
1856000
1856800
1857600
1858400
1859200
1860000
1860800
1861600
1862400
1863200
1864000
1864800
-2500
-2600
-2700
-2800
-2900
-3000
-3100
-3200
-3300
-3400
-3500
0
1000
2000
3000m

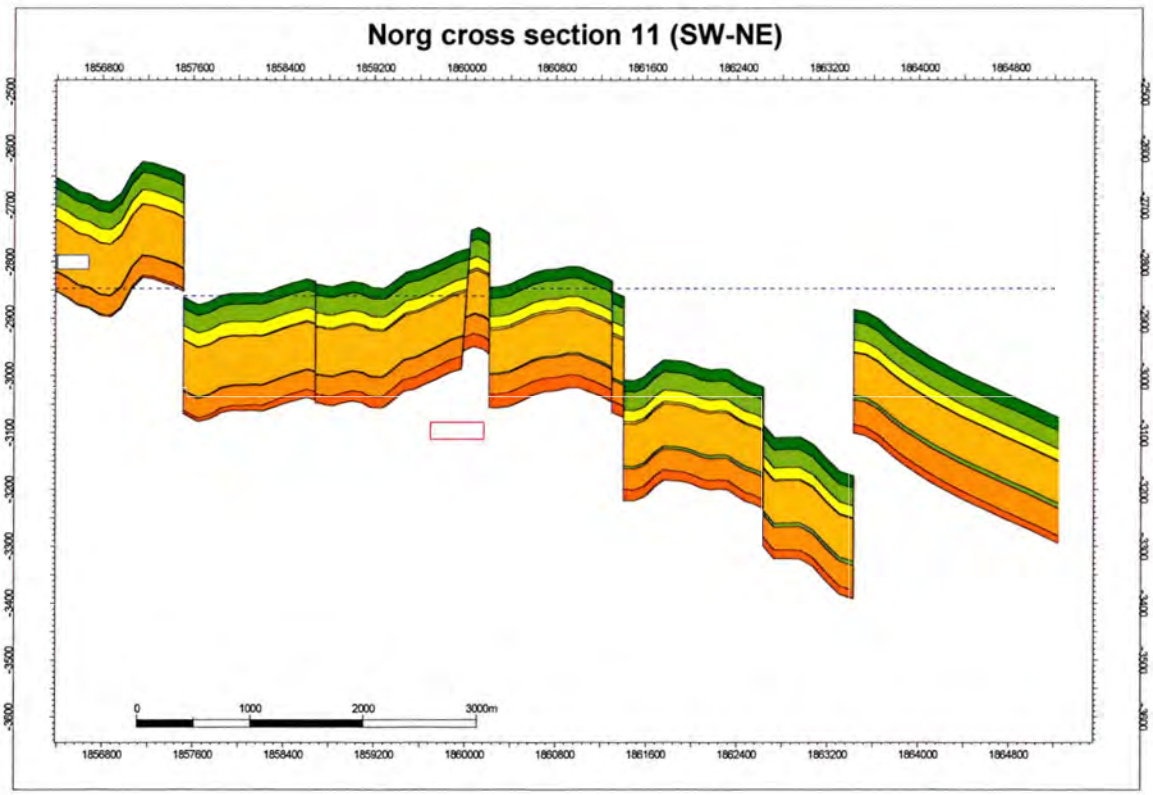
Norg cross section 11 (SW-NE)
1856800
1857600
1858400
1859200
1860000
1860800
1861600
1862400
1863200
1864000
1864800
-2500
-2600
-2700
-2800
-2900
-3000
-3100
-3200
-3300
-3400
-3500
-3600
0
1000
2000
3000m

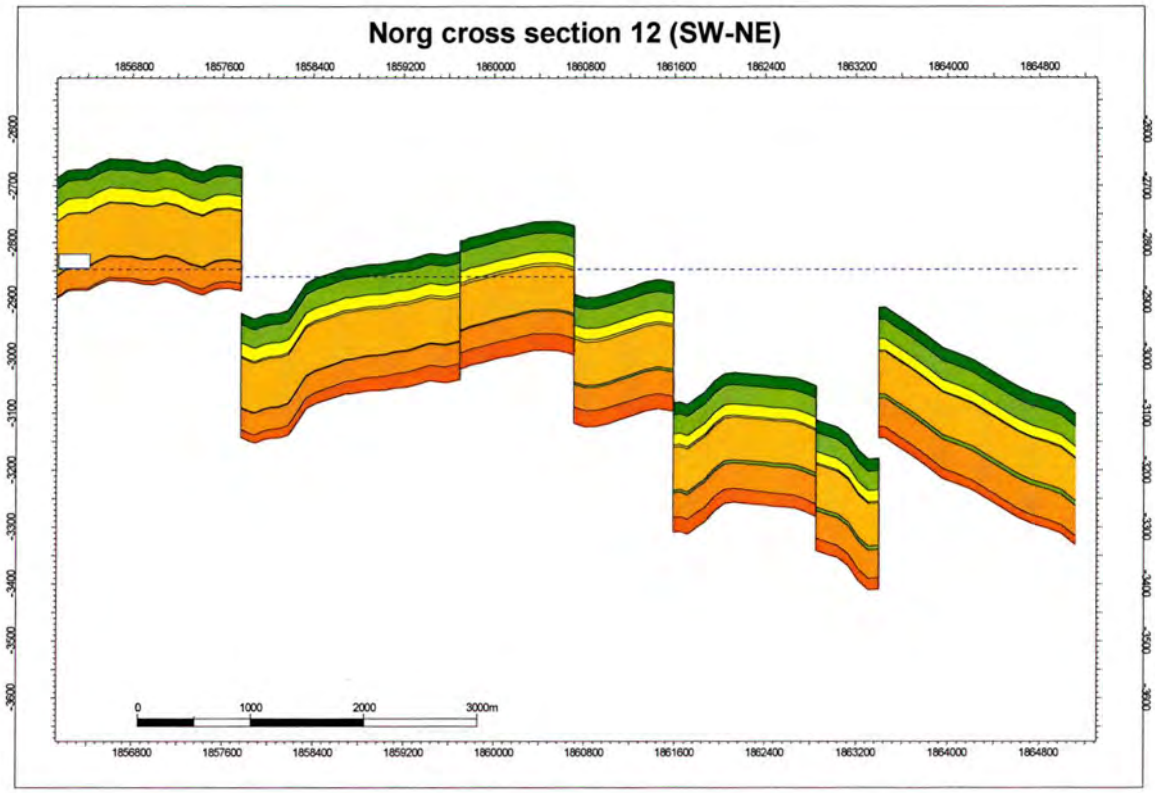
Norg cross section 12 (SW-NE)
1856800
1857600
1858400
1859200
1860000
1860800
1861600
1862400
1863200
1864000
1864800
-2600
-2700
-2800
-2900
-3000
-3100
-3200
-3300
-3400
-3500
-3600
0
1000
2000
3000m

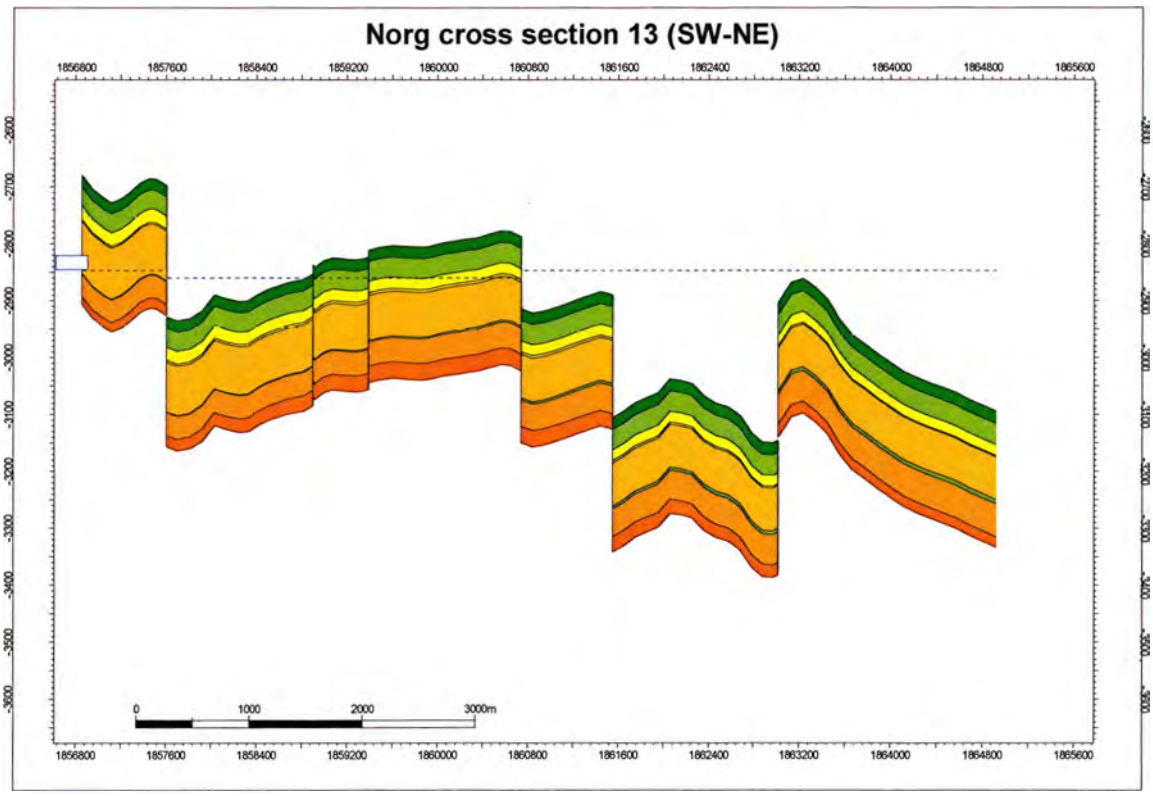
Norg cross section 13 (SW-NE)
1856800
1857600
1858400
1859200
1860000
1860800
1861600
1862400
1863200
1864000
1864800
1865600
-2600
-2700
-2800
-2900
-3000
-3100
-3200
-3300
-3400
-3500
-3600
0
1000
2000
3000m

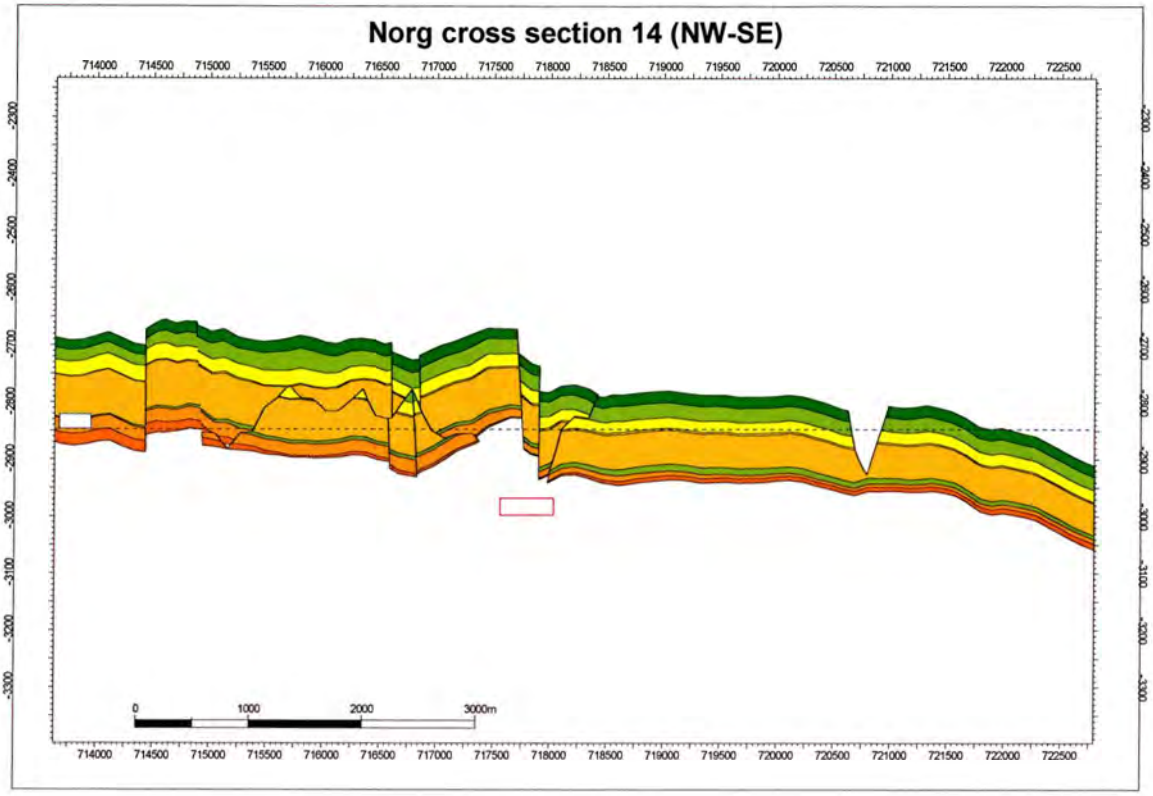
Norg cross section 14 (NW-SE)
714000 714500 715000 715500 716000 716500 717000 717500 718000 718500 719000 719500 720000 720500 721000 721500 722000 722500
-2300 -2400 -2500 -2600 -2700 -2800 -2900 -3000 -3100 -3200 -3300
0 1000 2000 3000m

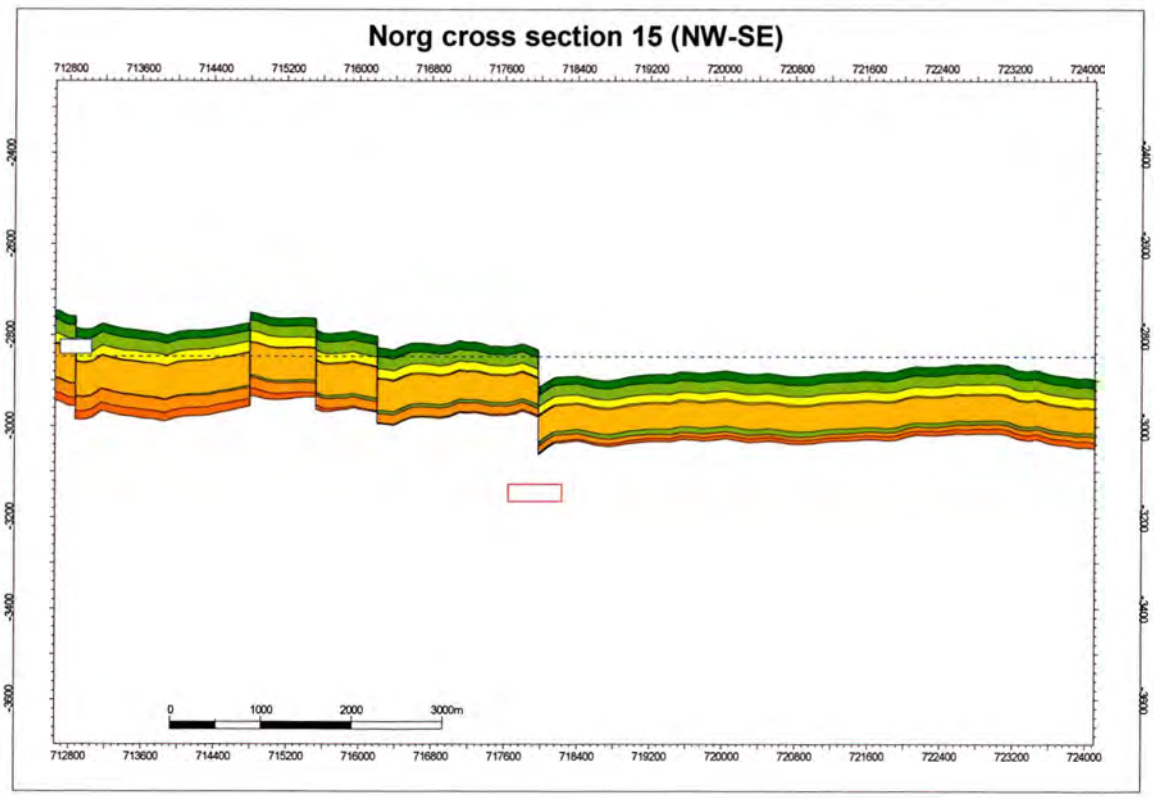
Norg cross section 15 (NW-SE)
712800 713600 714400 715200 716000 716800 717600 718400 719200 720000 720800 721600 722400 723200 724000
-2400 -2600 -2800 -3000 -3200 -3400 -3600
0 1000 2000 3000m

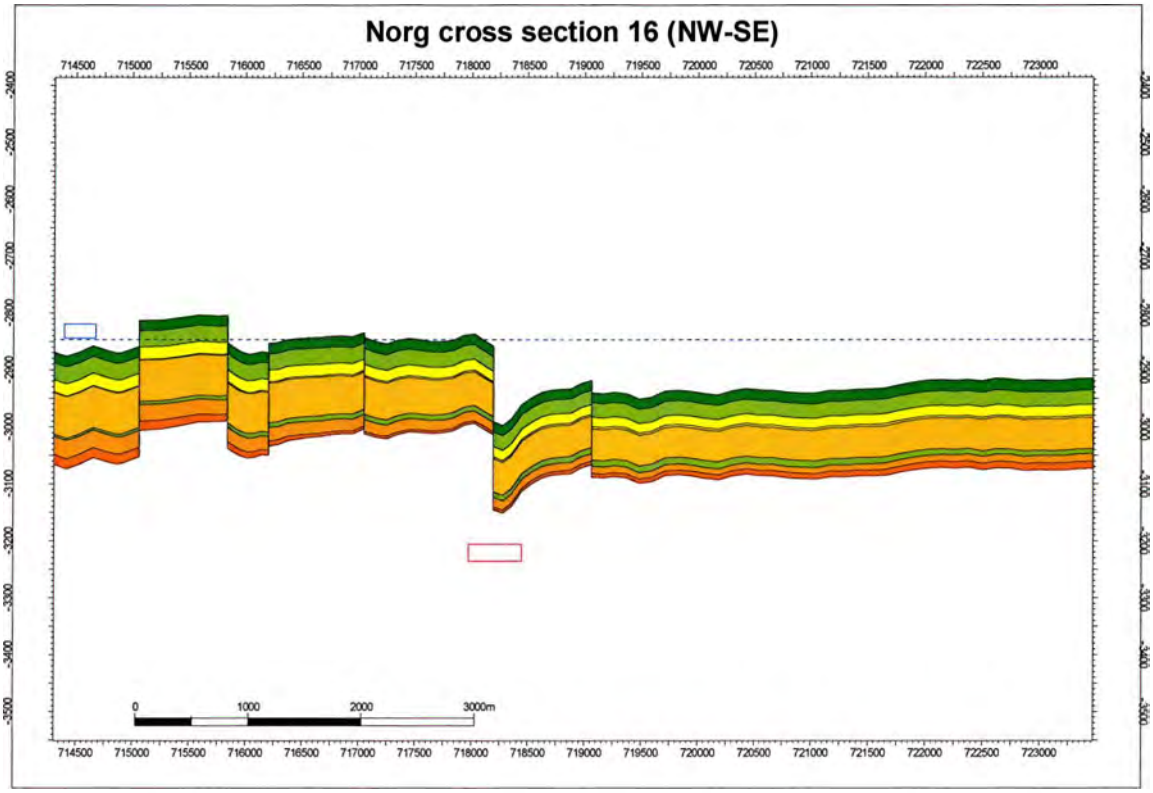
Norg cross section 16 (NW-SE)
714500 715000 715500 716000 716500 717000 717500 718000 718500 719000 719500 720000 720500 721000 721500 722000 722500 723000
-2400 -2500 -2600 -2700 -2800 -2900 -3000 -3100 -3200 -3300 -3400 -3500
0 1000 2000 3000m

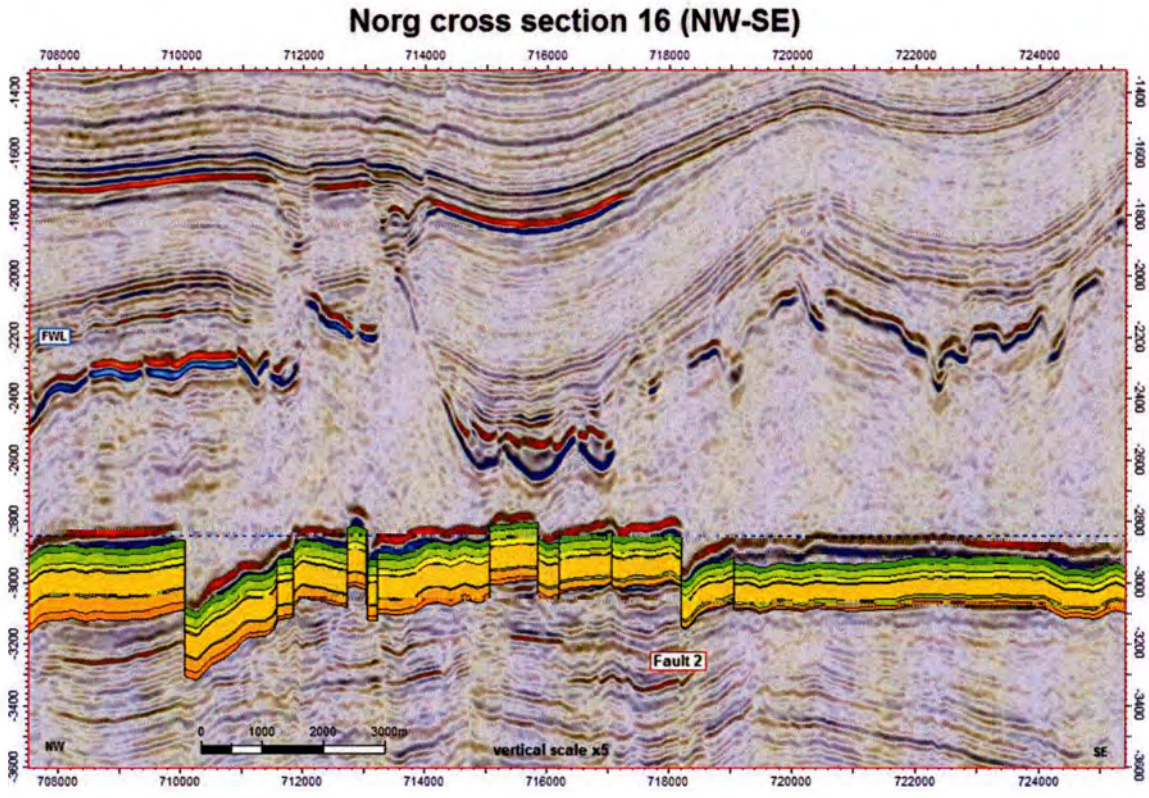
Norg cross section 16 (NW-SE)
708000 710000 712000 714000 716000 718000 720000 722000 724000
-1400 -1600 -1800 -2000 -2200 -2400 -2600 -2800 -3000 -3200 -3400 -3600
FWL
Fault 2
0 1000 2000 3000m
NW
vertical scale x5
SE

Enclosure-2 Residual friction coefficient

In this appendix, the impact of the residual friction coefficient on the fault slip response during depletion and subsequent re-pressurisation is evaluated. The cases in section 5.4.3 are repeated for a residual friction coefficient that is 0.10 lower than the initial friction coefficient rather than 0.15. The slope of the descending branch of the fault slip-weakening diagram is the same, namely $\Delta\mu$ = -0.0075 mm^{-1} (Table 13).

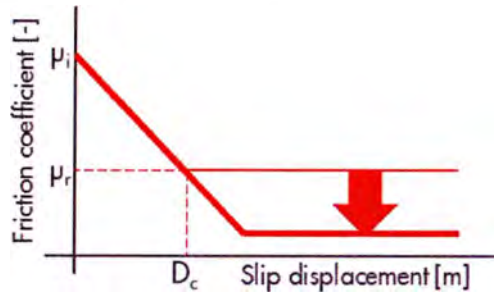

Table 13 Fault properties in the third series of analyses.

Run	Initial friction coefficient μ_i [-]	Residual friction coefficient μ_r [-]	Critical slip displacement D_c [m]	Slip-weakening gradient [mm^{-1}]	Depletion at onset of seismic rupture [MPa]
F2-31	0.20	0.10	0.0133	-0.0075	> 15.0
F2-32	0.22	0.12	0.0133	-0.0075	> 15.0
F2-33	0.24	0.14	0.0133	-0.0075	> 15.0
F2-34	0.26	0.16	0.0133	-0.0075	> 15.0
F2-35	0.28	0.18	0.0133	-0.0075	> 15.0
F2-36	0.30	0.20	0.0133	-0.0075	> 15.0
F2-37	0.32	0.32	0.0133	-0.0075	> 15.0

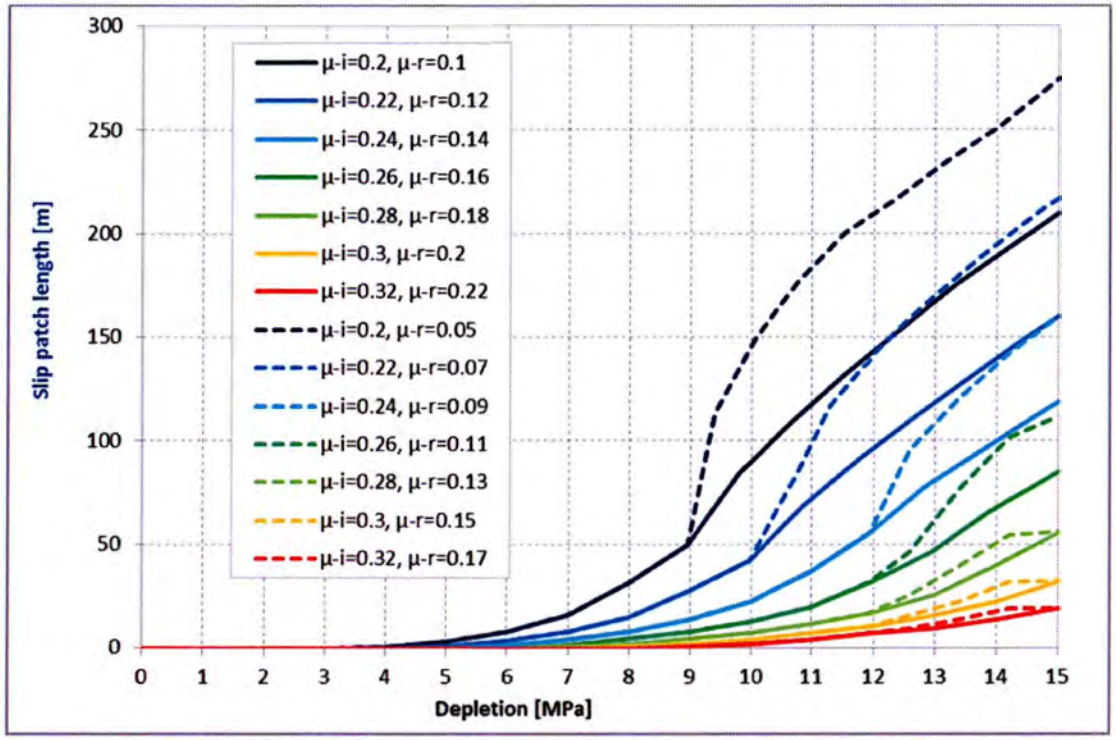

Figure 33 Length of the slip patch as a function of depletion for a reduction of the friction coefficient by 0.10 (solid lines), and for a reduction by 0.15 (dashed lines, same as Figure 30).

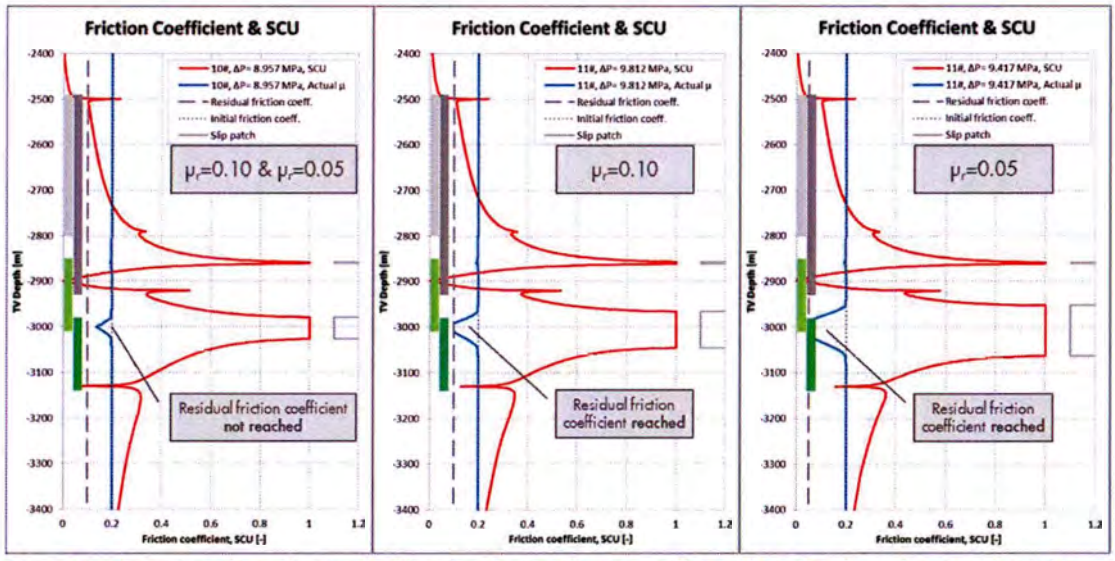

Figure 34 Shear Capacity Utilisation (red lines) and actual friction coefficient (blue lines) as a function depth for case F2-21 and F2-31 for 9 MPa depletion (left), 9.8 MPa depletion (case F2-31, middle) and 9.4MPa depletion (case F2-21 right).

Figure 33 shows that the slip patch length is independent of the residual friction coefficient until a certain depletion level for all cases. Comparing the dark blue lines for cases F2-21 (dashed) and F2-31 (solid) with an initial friction coefficient of 0.20, it is seen that the slip patch length is the same until about 9 MPa depletion. For the other cases with a larger initial friction coefficient, the deviation is less and starts at a higher depletion level.

This response is explained by the role of the residual friction coefficient, which limits the pace at which the slip patch grows with increasing depletion level. The left-hand graph in Figure 34 shows the SCU distribution (red line) and the actual friction coefficient (blue line) at 9 MPa depletion for case F2-31. The actual friction coefficient is equal to the initial value of 0.20 along most part of the fault, but drops below 0.20 over the slip patch where SCU=1, in accordance with the slip-weakening relationship. The minimum value of the actual friction coefficient at 9 MPa depletion is 0.155, while the residual friction coefficient in case F2-31 is 0.10 as indicated by the grey dashed line. Any residual friction coefficient smaller than 0.155 gives the same slip response at 9 MPa depletion, as long as the slope in the fault-slip weakening relationship is the same. This is the reason why case F2-21 yields the same slip response as case F2-31 despite the lower residual friction coefficient.

The middle and right-hand graph in Figure 34 show the condition at a somewhat higher depletion level, namely at 9.8 MPa depletion for case F2-31, and at 9.4 MPa depletion for case F2-21. The slip patch length for case F2-21 – with the smaller residual friction coefficient – is larger that case F2-31. Furthermore, the actual friction coefficient has dropped to the value of the residual friction coefficient over a part of the slip patch in both cases. This implies that over this area the fault strength does not reduce any further. A reduction in friction coefficient causes an acceleration of the slip patch length, whereas a constant (residual) friction coefficient provides stabilisation. This is taking effect beyond 9 MPa depletion for case F2-21 (Figure 33). The lower the residual friction angle, the later the stabilisation takes effect.

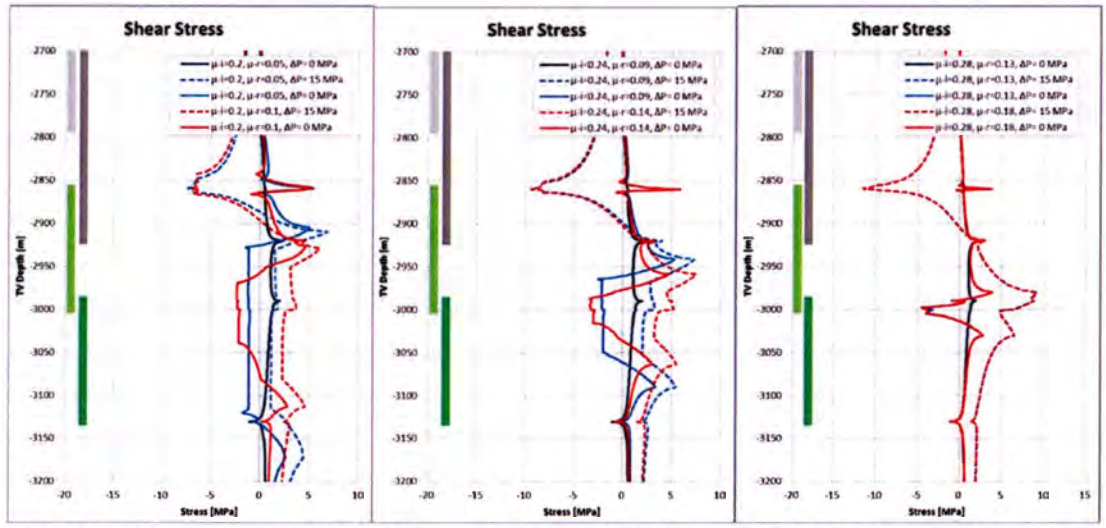

Figure 35 Influence of the residual friction coefficient on the shear stress distribution as a function of depth along the fault plane at 15 MPa depletion (dashed lines) and after re-pressurisation to virgin reservoir pressure (solid lines). Left: case F2-21 and F2-31. Middle: case F2-23 and F2-33. Right: case F2-25 and F2-35. Dark blue is the virgin shear stress condition.

Figure 35 shows the impact of the drop in friction coefficient for three values of the initial friction coefficient, namely for μ_i=0.20, 0.24 and 0.28 (from left to right). In each graph, a drop of the friction coefficient with 0.10 (light blue lines) and 0.15 (red lines) is compared. The dashed lines represent the shear stress at 15 MPa reservoir depletion, whereas the solid lines is the calculated stress distribution after the re-pressurisation stage (0 MPa depletion). The virgin reservoir pressure before depletion is given as reference (dark blue lines).

The shear stress distribution is the same if the friction coefficient drops with 0.10 or with 0.15 for an initial friction coefficient of 0.28 (right-hand graph). The slip displacement along the fault plane is too small to reach the critical slip displacement D_c (and thus the residual friction coefficient) for case F2-35 with the small drop in friction coefficient. So, it doesn't make a difference if a larger drop in friction coefficient is specified such as in case F2-25 (see also previous section). The same reasoning holds during the re-pressurisation stage.

The shear stress distribution is impacted by the residual friction coefficient for an initial friction coefficient of 0.24 at 15 MPa depletion (dashed lines, middle graph). In these two cases the residual friction coefficient is reached during the depletion stage, which explains why shear stress builds up higher for a larger residual friction coefficient (red dashed line). The difference in shear stress distribution becomes more pronounced after the re-pressurisation stage (solid lines, middle graph). The shear stress become smaller than the virgin shear stress (dark blue line) and reverses direction (negative values). The interval of more or less constant shear stress (solid lines) indicates the location and length of the slip patch after on depletion and re-pressurisation cycle. The slip patch is larger and the shear stress is smaller for a smaller residual friction coefficient. The differences become larger between a reduction in friction coefficient of 0.10 and 0.15 if the initial friction coefficient is 0.20 (left-hand graph). In particular the difference in length of the slip patch after a depletion and re-pressurisation cycle become larger.